TECHNISCHE UNIVERSITÄT WIEN
Vienna University of Technology

Inverter-Fed Estimation of Induction Machine Fundamental Wave Parameters at Standstill

Diplomarbeit

Ausgeführt zum Zwecke der Erlangung des akademischen Grades eines
Diplomingenieur (Dipl.-Ing.)

unter der Leitung von
Ao.Univ.Prof. Dipl.-Ing. Dr.techn. Thomas Wolbank

eingereicht an der
Technischen Universität Wien
Fakultät für Elektrotechnik und Informationstechnik
Institut für Energiesysteme und Elektrische Antriebe

von
Pesendorfer Christoph, BSc.
Matrikelnummer: 1225747

Wien, im Juni 2019

Arbeitsgebiet Elektrische Antriebe und Maschinen
Gußhausstraße 25-29/370-2, A-1040 Wien, Österreich
Internet: https://www.ieam.tuwien.ac.at

Abstract

Modern drive systems for induction motors (IM), require accurate knowledge of the motors equivalent circuit parameters. The control scheme in use, utilizes those to operate the IM. When the parameters are unknown but the motor is already connected to its load, conducting standard test might not be possible. Those tests also require trained personal, and thus are costly. In this thesis several identification methods which can be carried out at standstill are investigated. Additionally, the methods should be suitable for self commissioning. This means that they can be performed using a standard power inverter without any additional supply or measurement equipment. For each parameter one or more identification methods are studied in a simulation and with measurements. The stator resistance is identified with a DC-test. The transient inductance is found with a high frequency single phase test, a current and a voltage step test. For estimation of the magnetizing inductance a low frequency single phase test and a DC-decay test are investigated. The rotor resistance is identified with a single phase test and the rotor time constant is estimated with an iterative sinusoidal or flux observer based test. As each method has its advantages and disadvantages, the results of this thesis provide insight on their applicability.

Contents

List of Figures

Nomenclature

Symbols

i, I	...	current
u, U	...	voltage
φ	...	phase shift
r, R	...	resistance
x, X	...	reactance
z, Z	...	impedance
l, L	...	inductance
t	...	time
τ	...	time constant
f	...	frequency
ω	...	angular speed
Ψ	...	magnetic flux
ϑ, γ	...	space angle
p	...	number of pole pairs
T	...	mechanical torque
s	...	slip
n	...	rotational speed
σ	...	leakage factor
PF	...	power factor
G	...	transfer function
H	...	impulse response
h	...	step response
KP	...	proportional coefficient of a PI-controller
KI	...	integral coefficient of a PI-controller

Operators

j	...	imaginary unit
$Im\{\underline{z}\}$	...	imaginary part
$Re\{\underline{z}\}$	...	real part
$\lvert\underline{z}\rvert$	...	absolute value

Indices

S	...	stator
R	...	rotor
M	...	mutual/magnetizing
σ	...	leakage
m	...	mechanical
syn	...	synchronous
k	...	coordinate system
$'$	...	parameter of the inverse-Γ equivalent circuit
$S0$	...	constant value of a single phase vector
$S1$	...	amplitude of a single phase vector
N	...	rated value
ref	...	reference value
act	...	actual value
$meas$	...	measured value
U, V, W	...	phases of the three phase mains
$1, 2, 3$		

Reference Frames

α, β	...	stator fixed reference frame
d, q	...	rotor fixed reference frame
x, y	...	rotor flux reference frame

Acronyms

IM	...	induction motor
EC	...	equivalent circuit
PWM	...	puls width modulation
$SVPWM$	...	space vector puls width modulation
FOC	...	reference frame
RFO	...	field oriented control
DAQ	...	data acquisition
FFT	...	fast Fourier transform

CHAPTER 1

Introduction

Electric machines provide a way to transform electrical to mechanical energy or vice versa. From various types of electric machines, induction machines (IM) are the most common ones. [1] They are used in many industrial applications and can also be found in households or elevators. Although IMs can be used as generators and motors, their performance as motors is preferred. Advantages are the simple and robust structure, high durability, low maintenance effort and the relative low price. For simple tasks, the IM can also be run with direct connections to a three-phase system. The drawbacks are the high acceleration current and the low efficiency in comparison to synchronous motors. Since the emergence of power inverters the IM can also run at variable speeds, as the rotational speed is coupled with the supply frequency. [2, 3]
The use of 3-phase inverters also gave way to various control methods, with the most simple one being $V/f - control$. In feed forward control the flux inside the motor is kept constant. To reach different operating points, the voltage is varied in proportion to the frequency. Due to its poor dynamic speed performance, it is mostly used in simple applications. With the introduction of field oriented (or vector) control strategies, the dynamic performance was finally comparable to a synchronous machine. The so called rotor flux oriented control is widely used in high performance drive systems. Field oriented control systems require knowledge of the actual position of the flux linked with the rotor. The flux could be measured with hall sensors but this would increase the complexity and costs. Another option is to estimate the flux with the help of a rotary encoder and the electric quantities. Therefore, the rotor flux oriented (RFO) control requires accurate values of at least some IM parameters. Various RFO control schemes have been introduced throughout history. Which parameters are required depends on the applied RFO control scheme. [4] Running the system with control parameter values that do not match the actual values, results in a detuned operation. In modernizing projects or in cases where the motor and inverter are not sold as a unit, the parameters are not known beforehand. The parameters are then estimated during the drive initialisation. This process is also called self-commissioning. [5]

Numerous methods for IM parameter identification can be found in literature. Classical approaches are based on DC, locked rotor and no-load tests. [6] Where the no-load test requires the IM to rotate freely and the locked rotor test needs a locked rotor. In many applications the no-load test cannot be performed as the IM is connected to its load. Considering elevator modernizing, decoupling the load would be very difficult and cost intensive. In addition, trained personal is needed to conduct the classical tests. Hence, identifying the parameters at standstill is a more appropriate and economic approach. Parameter identification at standstill is also termed offline parameter identification.

Induction motor parameters vary with frequency, saturation and temperature and are only valid at a specific operating point. In some applications online identification is used which adjusts the control parameters during normal operation. Nevertheless, offline methods are investigated in this thesis.

1.1 Scope

This thesis investigates several induction motor parameter identification methods at standstill. These parameters are required for the field oriented control of the IM. The work for this thesis was performed in cooperation with Schindler Aufzüge AG in Corporate R&D Drives department in Ebikon, Switzerland. The goal is to evaluate methods, which can be implemented for self commissioning purposes. Self commissioning implies that the test can be conducted using only the inverter without any additional measurement or supply equipment. A complete identification process includes tests for all motor parameters that are required for the motor control. The reason for standstill identification is to either update or check existing parameters, or initialize an unknown machine. First, an extensive literature research was conducted where several fitting methods were chosen for further investigation. Apart from self commissioning a requirement is that the methods do not need excessive computational power and memory. Second the methods were simulated in MATLAB/Simulink and then experimentally verified using laboratory facilities of the R&D Drives department.

1.2 Structure

The second chapter starts by presenting the working principle of an induction motor. Then space phasors are introduced followed by the mathematical description of the IM including two equivalent circuits. At last the drive structure including the rotor flux oriented control and the features of three-phase voltage inverter are mentioned.

Chapter 3 provides an overview of standstill identification methods by first giving a general overview of state of the art methods found in literature. Second the principle of single phase excitation is explained. For each IM parameter the chosen methods for evaluation are then described in detail with their known up and downsides.

Chapter 4 shows the results of the parameter identification. The Matlab/Simulink environment is mentioned and the experimental setup is described. Then the results of the methods are presented in the same order as in chapter 3.

In the end Chapter 5 summarizes the results and findings of this thesis and suggests topics for future investigation.

CHAPTER 2

Induction Motor

This chapter provides a short summary about the mathematical formalism considering the induction motor. First, the working principle of an IM is explained and the different types are mentioned. Then an introduction in the space phasor theory is given, which is an important tool in describing the IM. After that, the most important equations are mentioned and two commonly used equivalent circuits are presented. At last, an outline of a common drive structure are introduced, with focus on the three phase inverter and the field oriented control scheme.

2.1 Principle of Operation

The induction motor produces its torque via electromagnetic induction. currents in the stator windings produce a rotating magnetic field. This field then induces a current through the rotor windings. Together, the rotor currents and the stator field are responsible for the creation of torque. An IM always rotates slower than the produced stator field. If the rotor would move at the same speed, the field seen from the rotor would be constant. Leading to a vanishing rotor current and torque.[5] The absolute and relative difference in angular speed are called slip frequency ω_{slip} and slip s.

$$\omega_{slip} = \omega_{syn} - \omega_m \tag{2.1}$$

$$s = \frac{\omega_{syn} - \omega_m}{\omega_{syn}} \tag{2.2}$$

where ω_m is the mechanical speed of the rotor and ω_{syn} is the synchronous angular speed of the stator field. The synchronous angular speed is determined by the electric frequency f and the number of pole pairs p:

$$\omega_{syn} = \frac{2\pi f}{p} \tag{2.3}$$

IMs are mainly categorized into two groups depending on the type of the rotor windings. Squirrel-cage motors have embedded bars as windings in the rotor slots which are short circuited at both ends. Wound rotor types contain a three phase winding on the rotor similar to the stator. [1] Wound types produce a smoother torque whereas squirrel-cage motors are more economic and simpler to manufacture. In this thesis the focus lies on the squirrel-cage type. Nevertheless, the methods could also be applicable for IMs with wound rotors.

2.2 Space Phasor Theory

The Space Phasor Theory was first introduced 1959 by Kovács [7] and is now commonly used to model the transient conditions of a motor. In principle, the spatial distribution of the electric and magnetic quantities inside of the machine are represented with a space phasor in the complex plane. The theory provides an elegant way to depict the transient conditions of electric machines and simplifies their control strategies. For its application, the following simplifying assumptions need to be made:

- The machine structure is rotationally symmetrical
- The 3-phase supply network is symmetrical
- Electromagnetic quantities are sinusoidally distributed along the machines radius. Therefore only the first harmonic will be taken into account.
- The machine parameters are assumed to be constant. Varying resistances or saturation must be set according to the operating point

With the assumptions above, the spacial distributed magnetic potential inside the air gap is sinusoidal. The current space phasor is then defined in a way that it always points to the maximum of the magnetic potential. This space phasor defines the current state of the machine and can be transformed back into the phase currents unambiguously. The three phase currents are transformed using the so called Clark Transformation.

$$\underline{i}_{\alpha,\beta} = \frac{2}{3} \cdot (i_U + i_V \cdot \underline{a} + i_W \cdot \underline{a}^2) \tag{2.4}$$

with:

$$\underline{a} = e^{j\frac{2\pi}{3}} \tag{2.5}$$

The Clark Transformation can also be applied to the voltage and flux without any restrictions:

$$\underline{u}_{\alpha,\beta} = \frac{2}{3} \cdot (u_U + u_V \cdot \underline{a} + u_W \cdot \underline{a}^2) \tag{2.6}$$

$$\underline{\psi}_{\alpha,\beta} = \frac{2}{3} \cdot (\psi_U + \psi_V \cdot \underline{a} + \psi_W \cdot \underline{a}^2) \tag{2.7}$$

This transformation can also be reversed. The phase quantities are calculated as shown here for the current:

$$i_u = Re\{\underline{i}_S\} \tag{2.8}$$

$$i_v = Re\{a^2 \cdot \underline{i}_S\} \tag{2.9}$$

$$i_w = Re\{a \cdot \underline{i}_S\} \tag{2.10}$$

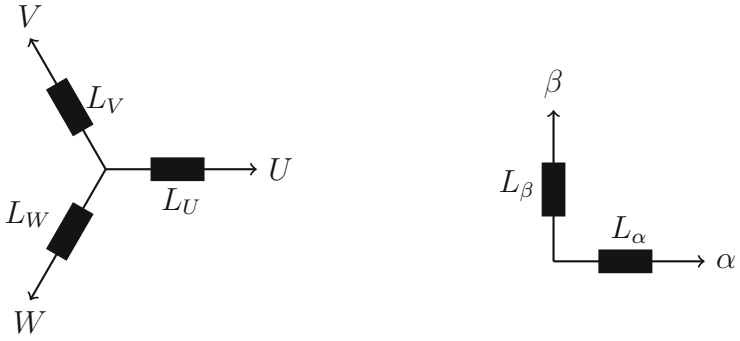

Figure 2.1: The three phase system on the left gets transformed into the 2 phase system shown on the right side.

In the field oriented control of electric machines, the space phasors are needed in different Reference Frames (RF) or coordinate systems. The three most common ones are described below. Although the transformations between the reference frames are given for the current phasor, they can also be used for all space phasors. In figure 2.2 all 3 mentioned reference frames are displayed with respect to a randomly chosen rotor flux space phasor.

Stator reference frame (α, β) The real and imaginary part of equation (2.4) represent the stator RF. This RF is fixed to the stator. The α-axis points in the direction of phase u.

Rotor reference frame (d, q) This RF is fixed to the rotor and therefore moves with mechanical angular speed ω_m in relation to the stator RF. Quantities in the (d, q)-RF are calculated using the mechanical rotor angle γ_m.

$$\underline{i}_{d,q} = \underline{i}_{\alpha,\beta} \cdot e^{-j\gamma_m} \tag{2.11}$$

Synchronous reference frame (x, y) This RF is fixed to the rotor flux and by definition, the rotor flux points towards the x-axis. In relation to the stator RF it rotates with the synchronous angular speed ω_Ψ. Quantities in the (x, y)-RF are calculated using the synchronous rotor angle γ_Ψ.

$$\underline{i}_{x,y} = \underline{i}_{\alpha,\beta} \cdot e^{-j\gamma_\Psi} \tag{2.12}$$

It should also be mentioned here that in English literature, the synchronous reference frame often is termed dq-RF.

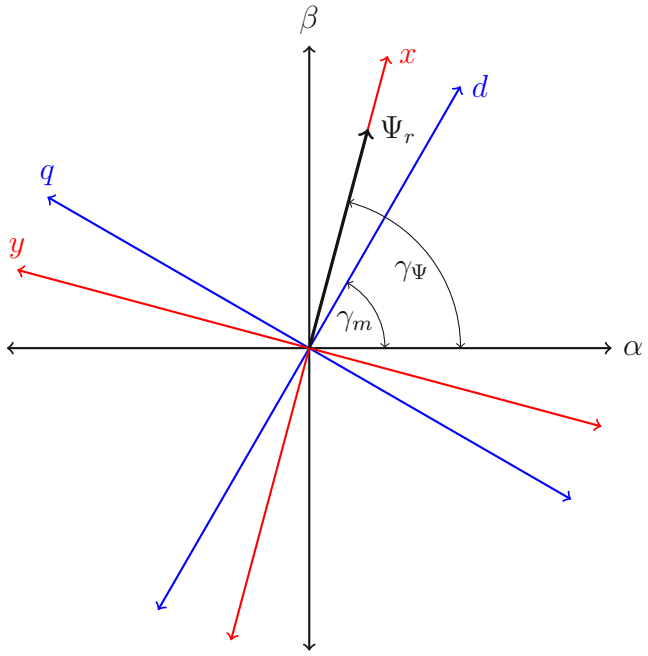

Figure 2.2: The stator(α, β), rotor (d, q) and synchronous (x, y) reference frame with respect to the rotor flux space phasor Ψ_r.

2.3 Mathematical Model & Equivalent Circuits

This section provides the mathematical model of an induction machine with respect to [8] and the use of the space phasor theory, described in the previous section. Furthermore, two equivalent circuits of the induction machine are introduced in the subsections.

In a general reference frame, rotating with the angular speed ω_k, the IM can be described by the following equations:

Stator Voltage Equation

$$\underline{u}_S = \underline{i}_S \cdot R_S + \frac{d\underline{\Psi}_S}{dt} + j\omega_k \underline{\Psi}_S \tag{2.13}$$

where $\underline{u}_S$ is the voltage seen at the stator terminals, $\underline{i}_S$ the stator current, R_S represents the stator winding resistance and $\underline{\Psi}_S$ is the stator flux. The subscript S stands for "stator".

Rotor Voltage Equation

$$\underline{u}_R = \underline{i}_R \cdot R_R + \frac{d\underline{\Psi}_R}{dt} + j(\omega_k - \omega_m)\underline{\Psi}_R \tag{2.14}$$

where: $\underline{u}_R$ is the rotor voltage, $\underline{i}_R$ the rotor current, R_R represents the rotor resistance and $\underline{\Psi}_R$ is the rotor flux. The subscript R stands for "rotor". In case of a squirrel cage motor, the rotor circuit is short circuited and $\underline{u}_R = 0$ As in this thesis only this type of motor is considered, $\underline{u}_R$ is always zero.

Stator Flux Equation

$$\underline{\Psi}_S = L_S \cdot \underline{i}_S + L_{SR} \cdot \underline{i}_R \tag{2.15}$$

where: L_S is the stator inductance and L_{SR} the mutual inductance of the rotor and the stator circuits

Rotor Flux Equation

$$\underline{\Psi}_R = L_R \cdot \underline{i}_R + L_{SR} \cdot \underline{i}_S \tag{2.16}$$

where: L_R is the rotor inductance.

Based on the equations above, and using a turns ratio similar to that used for transformers, an induction machine can be modelled with various equivalent circuits. Two EC are described below.

Torque Equation

$$T = -Im\{\underline{i}_S * \underline{\Psi}_R\} \tag{2.17}$$

The resulting torque T of the motor is calculated with the imaginary part of the stator current times the rotor flux.

2.3.1 T - Equivalent Circuit

By applying a turns ratio, similar to a transformer the rotor quantities can be referred to the stator side. Hence the IM can be described with an equivalent circuit. The stationary T - equivalent circuit, shown in 2.3 is very commonly used and often referred to as the standard induction motor EC. [9] [10] On the rotor side of the circuit, $\frac{R_R}{s}$ represents the mechanical load of the motor, as the slip s is dependent on the torque. $L_{\sigma S}$ and $L_{\sigma R}$ are the stator and rotor leakage inductances. L_M is the mutual inductance. These inductances are defined as follows:

$$L_S = L_{\sigma S} + L_M \tag{2.18}$$

$$L_R = L_{\sigma R} + L_M \tag{2.19}$$

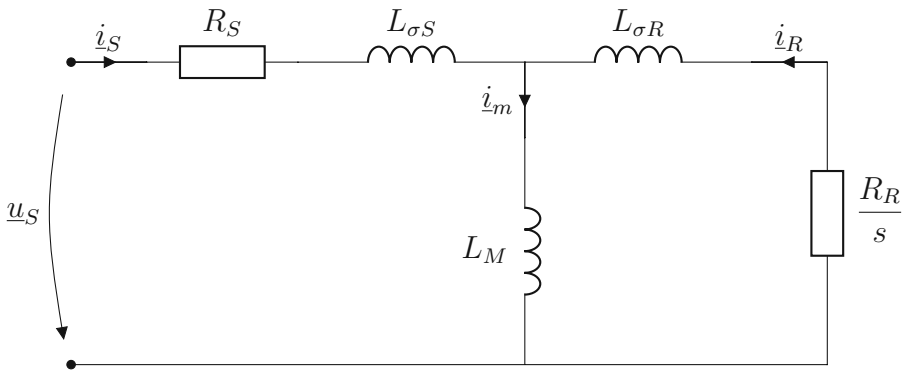

Figure 2.3: Stationary T-Equivalent Circuit

2.3.2 Inverse Γ-Equivalent Circuit

Using a different turns factor the stator and rotor leakage inductance can be referred to the stator side using the below introduced leakage factor σ, the stationary EC can be redrawn to the inverse Γ-circuit.

$$\sigma = 1 - \frac{L_M^2}{L_S \cdot L_R} \tag{2.20}$$

In the circuit shown in figure 2.4, it can be seen that this reduces the amount of parameters to four. This circuit is most commonly used in the parameter standstill estimation, as it is only necessary to estimate four parameters. In addition to simplicity, the leakage inductance or transient inductance σL_S is required for the current controller in the rotor flux oriented control scheme. A detailed explanation of this control structure is given in the next chapter.

The referred parameters are calculated as follows.

$$R'_R = R_R \cdot \frac{L_M^2}{L_R^2} \tag{2.21}$$

$$\underline{i}'_R = \underline{i}_R \cdot \frac{L_M}{L_R} \tag{2.22}$$

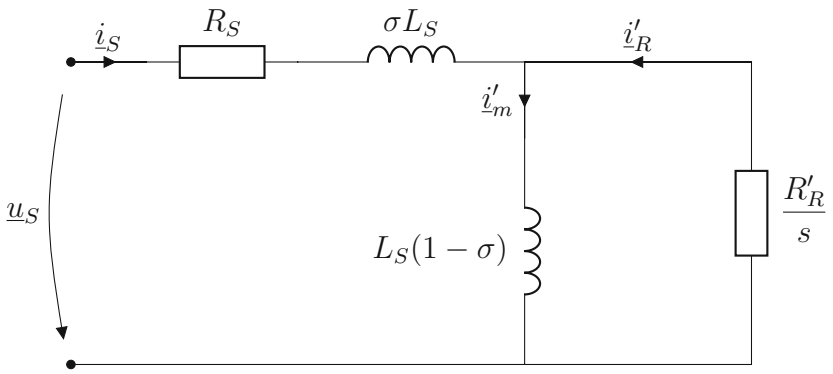

Figure 2.4: Stationary Inverse Γ -Equivalent Circuit

Parameter Conversion For completeness the formulas to convert the inverse-γ parameters to the standard values are given here. At first the total leakage inductance needs to be split into the rotor and the stator leakage inductance. As recommended by IEEE [9] the NEMA design type of the motor is used to calculate $L_{\sigma S}$ and $L_{\sigma R}$. If the NEMA type is unknown, two leakage inductances are assumed to be equal. Therefore,

$$L_{\sigma S} = L_{\sigma R} = \frac{\sigma L_S}{2} \tag{2.23}$$

the mutual inductance is then determined by,

$$L_M = \frac{L_S}{2} \cdot (2 - \sigma) \tag{2.24}$$

ans the rotor inductance and the rotor resistance can be calculated with,

$$L_R = \frac{L_M^2}{(1-\sigma)L_s} \tag{2.25}$$

$$R_R = R'_R \cdot \frac{L_R^2}{L_M^2} \tag{2.26}$$

2.4 Drive Structure

A simple drive structure consist of a power inverter an induction motor and the load. The inverter gets supplied from the mains and converts the voltages to the desired values. These are applied to the IM which is then able to produce torque. The inverter also possesses a control unit, which sets the PWM switching times and processes any measurements. Measured quantities are commonly the DC-Link voltage, the output phase currents, the IM speed and temperature.

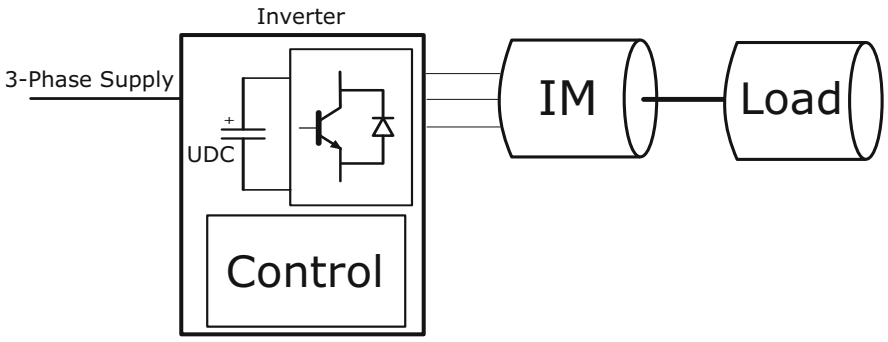

Figure 2.5: This figure shows a simplified version of an induction motor drive structure.

2.4.1 Rotor Flux Oriented Control

Apart from other methods like the direct torque control, the rotor flux oriented control is very widely used. The parameter identification in this thesis focuses especially on the estimation of the parameters required for the rotor flux oriented control for a speed drive. Therefore, this control scheme is introduced here and the required parameters are briefly discussed.

RFO control utilizes the idea, to control the torque and flux in the machine separately. The synchronous reference frame, mentioned in 2.2 which rotates with the rotor flux at the synchronous frequency is used. As the y-component of the rotor flux is per definition zero, the following equations can be derived from 2.13-2.17 for the inverse-Γ equivalent circuit. [11]

$$\tau_R \frac{d\Psi_R}{dt} + \Psi_R = (1-\sigma) L_S \cdot i_{s,x} \tag{2.27}$$

$$\omega_{slip} \tau_R \Psi_R = (1-\sigma) L_S i_{s,y} \tag{2.28}$$

$$T = \frac{3}{2} \frac{p}{\sigma L_S} \Psi_R \cdot i_{s,y} \tag{2.29}$$

The stator currents x component, which points in the same direction of the flux builds up the rotor flux. Whereas the y component directly influences the torque. Although both components could be used to control the torque, $i_{s,x}$ and therefore the flux is kept constant as 2.27 represents a first order delay element. Instead of Ψ_R the magnetizing current i'_m, shown in figure 2.4, can be utilized in the equations above.

$$\Psi_R = (1-\sigma) L_S \cdot i'_m \tag{2.30}$$

As the direction of the flux is normally not measured directly, it needs to be estimated using the motor parameters and the measurements provided by the inverter. A vector controlled induction motor can be used within a torque drive, a speed drive, or a position drive. The type of the drive that exhibits the highest sensitivity to the incorrect parameter values is the torque drive. Although the motor parameter variations affect the speed control applications too, existence of the PI speed controller considerably reduces negative consequences of the parameter detuning.[4] Many different forms of flux observers can be found in literature where the rotor time constant is an important parameter. To get the desired currents, a current controller is used in the x-y reference frame. For the tuning of the PI current controller knowledge of σL_S is necessary. $(1-\sigma)L_S$ needs to be known for the field weakening.

2.4.2 Three Phase Inverter

In the later proposed identification techniques, the IM is fed by a three phase inverter, as it would be impractical and expensive to use extra test equipment. The structure of three phase inverter is shown in figure 2.6. First the 3-phase grid supply $U_1 - U_3$ is converted to a DC voltage V_{DC} that is smoothed by the DC-link capacitor. Then, the output circuit sets the desired voltage via pulse width modulation(PWM).

Non-Linearities The measurements for the parameter identification, should also be taken from the inverter without the use of any additional measurement equipment. As mentioned only the phase currents and the DC-link voltage are commonly measured. Therefore, the voltage at the load terminals is reconstructed by means of the DC-link voltage and the PWM switching duty cycles. It can be derived from figure 2.6 that the real voltage at the load terminals(U_U, U_V, U_W) differs from the calculated one due to the characteristics of the semiconductor devices. The effects of the semiconductors lead to a non-linear voltage gain and are referred to as inverter non-linearities They consist mainly of:

1. The semiconductor threshold voltage

2. The on-state resistance caused by the switches and diodes when conducting [12]

3. Blanking time
   To prevent a DC-link short-circuit, the switch pairs for each phase (1/4, 2/5 and 3/6) are not allowed to conduct at the same time. As the switches have a finite switching time, a short delay is added to the turn-on switch command. This delay is also called shoot-through delay. [13][14][15]

4. The output voltage transition slope. [11]

Whereas, the third and forth effects are usually mentioned together as dead time effects. The overall effect of inverter switches appears as a voltage drop at the switches, which is a non-linear function of the current through the switches. And therefore, leading to the error between the set voltage and the actual voltage appearing across the load terminals.

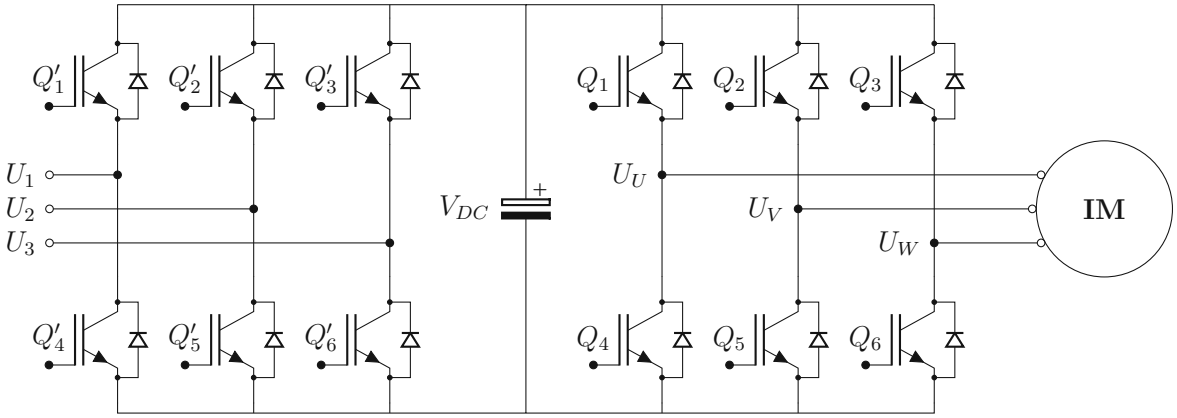

Figure 2.6: Three-phase inverter with a DC link capacitor and 6 antiparallel IGBT Diode pairs. $Q'_1 - Q'_6$ define the input and $Q_1 - Q_6$ the output circuit. The induction motor (IM) is symbolized by the circle on the right and the mains supply is represented by $U_1 - U_3$.

CHAPTER 3

Parameter Identification Methods

To characterise the parameters of an induction motor, the IEEE standard [9] provides guidelines using the standard no-load and locked rotor test. These tests however are only fit for laboratory conditions with stable ambient conditions as well as precise measuring instruments and data acquisition systems. Modern electric drive systems with powerful on-board computational capabilities can eliminate the need for the elaborate standard tests. [6] Identification of motor parameter, prior to normal operation is known as offline identification. Online estimation on the other hand tracks and updates the parameters during operation. Offline parameter identification can be classified in three broad categories. The first one uses numerical analysis tools without any measurements. Parameters are obtained from manufacturer data such as geometric dimensions and by solving analytical equations. [16, 17] For the second one free rotation of the rotor shaft is required which might not be possible due to application limitations. Suspect of investigation in this thesis is the third one. Thereby all the tests are performed at standstill. The equivalent circuit parameters are estimated by applying different excitation signals through the inverter. Signals from DC to high frequency AC can be generated. If the tests do not require locking of the rotor or any additional equipment they can be further termed as self-commissioning. For AC signals, single phase excitation which does not produce any torque is often the supply of choice. Single phase supply is described in detail in 3.2 Self commissioning of an IM implies the following conditions.

1. The motor must not rotate.
   Resulting in $\omega_m = 0$ and $s = 1$ when $\omega_{syn} > 0$

2. Measurements are only taken from standard drive system sensors
   Meaning only the currents and the DC-Link voltage.

3. Calculations can be made using only the inverter

Out of the many methods available, only the ones which are suitable for self commissioning and do not require excessive computational power are considered for investigation. Now a short overview about state of the art methods is given which is followed by

introducing single phase excitation. Then the studied methods for the equivalent circuit parameters identification sorted by the parameter, are described in detail.

3.1 State of the Art

Many different standstill identification methods have been proposed in literature. Only the ones which use the inverter to generate the test signals are considered. In [18],[19] a DC voltage or current is used to estimate the stator resistance. The rotor resistance referred to the stator is obtained through a rapid current reversal test in [18]. A fast current ramp or voltage pulse is applied to estimate the transient inductance in [11]. The magnetizing inductance can be found using a low frequency single phase excitation in [20] or a DC decay test as in [21]. All these tests use single phase excitation to be suitable for self commissioning. [22] and [23] recommend supplying the motor at two different frequencies and using an iterative calculation to obtain the inductances. Standstill variable frequency response tests are proposed in [19]. In [24] the identification process uses a single phase supply and the solving of several integrals. Adaptive linear neural networks are employed for standstill parameter estimation in [25] and [26]. [27] introduces an identification method using the frequency characteristics of rotor bars. By measuring the stand sill frequency response of the IM and using a curve fit of an analytical model, [28] estimates the parameters. Additional methods are mentioned in [6] which provides an up to date technology status review.

3.2 Single Phase/Axis Excitation

To satisfy the requirements on self-commissioning a great number of methods found in literature identifies the parameters by means of single phase or single axis tests. The benefit of these tests is that the rotor does not need to be locked. No torque is produced and the behaviour of the machine is almost the same as with three phase excitation. [22] Hence, these methods are suitable for many applications in which locking the rotor may not be possible.

When operating within the linear range there is no severe difference related to the electric behaviour of the machine at three- and single-phase excitation. Only in the saturation range at the three-phase excitation, the magnetizing inductance is slightly larger than that in the case of single phase excitation.This effect is due to third order harmonics, which appears at three-phase excitation in the winding voltages. These harmonics counter-work the sources of saturation and as a consequence the effective magnetizing inductance is slightly larger than in the case of single- phase excitation, where such harmonics can not occur. [29]

In single axis tests, the inverter sets a sinusoidal voltage space phasor with a constant space angle ϑ via space vector modulation. As a result, the current and flux space phasors point in the same direction and do not rotate over time. Therefore no torque is

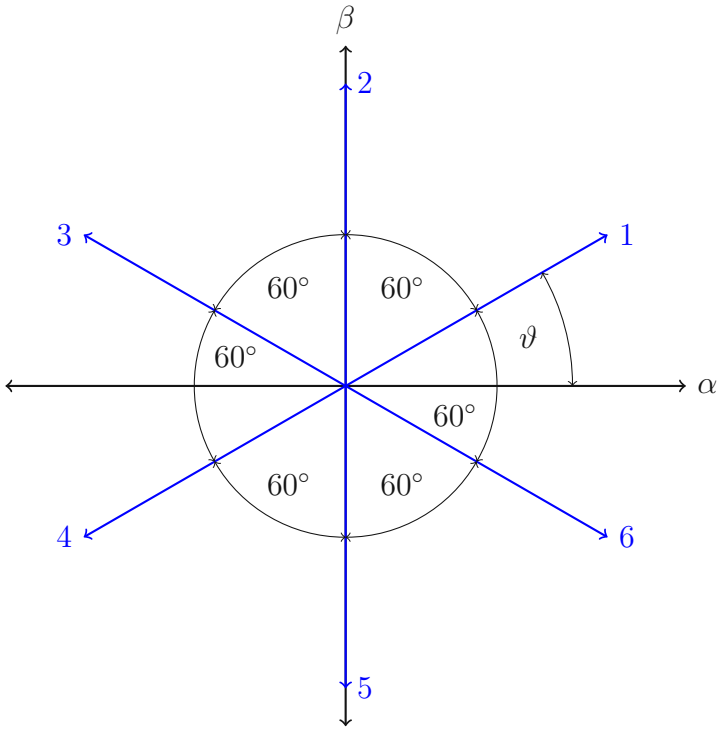

Figure 3.1: This figure shows the 6 possible voltage or current space phasor directions $(1-6)$ in single phase tests.

generated. The single phase voltage and current space phasors, are described as:

$$\underline{u}_s(t) = (U_{S0} + U_{S1}cos(\omega t))e^{j\vartheta} \tag{3.1}$$

$$\underline{i}_s(t) = (I_{S0} + I_{S1}cos(\omega t))e^{j\vartheta} \tag{3.2}$$

For any chosen space angle the method is termed single axis.
In a single phase test, only 2 phases are conducting. This can be achieved by disconnecting one phase which does not fit the term self-commissioning though. Another approach is to set the voltage space phasor to one of the 6 directions, shown in figure 3.1. By inserting a space phase with an angle of $\vartheta = 30°, 90°, 150°, 210°, 270° or\ 330°$ into the equations 2.8-2.10 this can easily be proven.

3.3 Nameplate Data Estimation

The nameplate of an IM specifies several quantities of the machine. With those values, initial estimates of the equivalent circuit parameters can be made. Only R_S cannot be estimated. Those estimates are inaccurate but can be used to find e.g. injection frequencies for the proposed identification methods. Apart from other data, the quantities shown in Table 3.1 are usually stated on a nameplate. Depending on the way the IM is connected (star or delta) the rated voltage or current needs to be divided by $\sqrt{3}$ to get the phase value.

Rated Voltage $U_N[V]$
Rated Current $I_N[A]$
Rated Speed $n_N[Rpm]$
Rated Frequency $f_N[Hz]$
Power $P[W]$
Power Factor$(cos(\varphi))$ $PF[1]$

Table 3.1: Motor quantities usually stated on a machines nameplate.

In some cases, the number of pole pairs is also given. If not, the speed and frequency are used in the equation below. The rated mechanical speed is lower than the synchronous speed due to the slip. Therefore $\frac{f_N}{n_N}$ needs to be rounded down to the next integral number.

$$p = rounddown(\frac{f_N}{n_N}) \tag{3.3}$$

Knowing the number of pole pairs, the synchronous angular speed and therefore the rated slip can be obtained.

$$s_N = \frac{\omega_{syn} - \omega_{mN}}{\omega_{syn}} \tag{3.4}$$

Now a rough simplification is made to the equivalent circuit. The leakage inductances and the stator resistance in 2.3 are neglected resulting in an EC inhibiting L_M in parallel with R_R/s. Knowing the IM rated current and power factor the current though each branch is calculated.

$$I_R = I_N \cdot cos(\varphi) \tag{3.5}$$

$$I_M = I_N \cdot sin(\varphi) \tag{3.6}$$

Further using the rated slip and the rated voltage from the nameplate, the values of R_R and L_M are computed.

$$L_M = \frac{U_{N,phase}}{2\pi \cdot f_N \cdot I_M} \tag{3.7}$$

$$R_R = \frac{U_{N,phase} \cdot s_N}{I_R} \tag{3.8}$$

To estimate the leakage inductances, the starting current of the machine is assumed to be 5 times the rated current. Further assuming that the voltage drop over the stator and rotor resistance is negligible during start up and that the magnetizing inductance is too large to permit rapid current rise. The equivalent circuit is reduced to the two leakage inductances in serial.

$$L_{\sigma S} + L_{\sigma R} = \frac{U_{N,phase}}{2\pi \cdot f_N \cdot 5 \cdot I_N} \tag{3.9}$$

As already mentioned, separately acquiring the leakage inductances is a difficult task and therefore they are often assumed to be equal.

3.4 Stator Resistance

The stator resistance R_S is most widely identified by means of a DC test. [30, 19, 31, 32, 21, 33] Other methods such as, a single phase test at two frequencies or a frequency response curve fit as in [28] are not considered here, since the DC test is simple and provides accurate results. Obtaining the parameter is generally a basic requirement for the estimation of other motor parameters. [19] R_S is often used to tune the current controller and is needed for some flux observer models. This parameter varies with the temperature since it represents the actual resistance of the stator windings. Nevertheless R_S is obtained at room temperature and will further be considered constant. To identify the stator resistance, an appropriate constant current is applied to the stator. With DC supply the flux inside the motor is also constant and 2.13 in the stationary reference frame is reduced to:

$$\underline{U}_S = \underline{I}_S \cdot R_S \tag{3.10}$$

In standard drive systems only the current is measured and the voltage is reconstructed using the DC-link voltage and the PWM switch commands. Therefore the voltage drops over the IGBTs need to be taken into account. To compensate for the inverter non linearities, the measurement is taken at two DC current levels. The non linearities can be considered as constant for these two measurements if the voltage is high enough. Using the difference between the two voltage-current pairs the resistance is calculated with:

$$R_S = \frac{|\underline{U}_{S2}| - |\underline{U}_{S1}|}{|\underline{I}_{S2}| - |\underline{I}_{S1}|} \tag{3.11}$$

Figure 3.2 displays this method where it can be observed that the voltage and current measurements need to be taken after the voltage reaches a steady state.

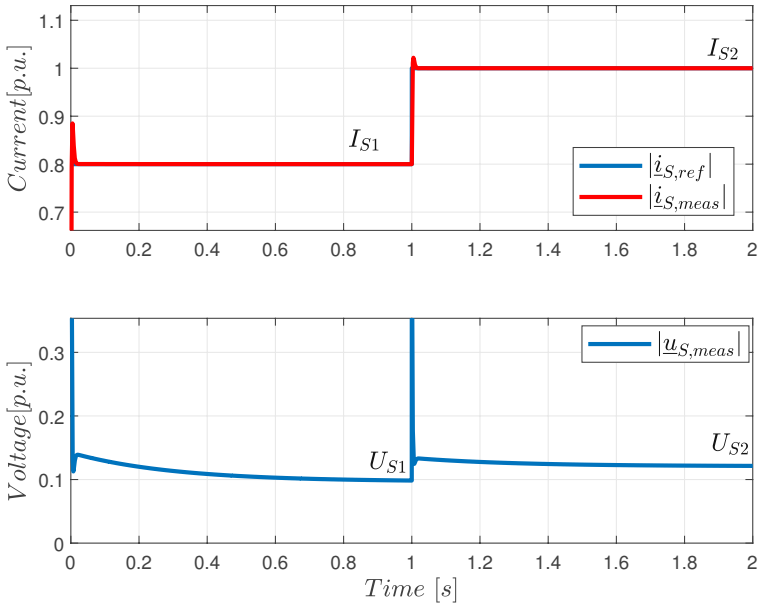

Figure 3.2: Stator resistance DC-test recorded in simulink.

As the current should be high enough to assume constant inverter non linearities for the two tests, the test should be as short as possible to not produce excessive heating in the stator windings. In order to improve accuracy, the measurements are conducted at three different space angles ϑ and their mean value is taken. A good approach would be to use e.g. $30°, 90°, 150°$ since only 2 phases will be conducting at a time.
Though the test could also be performed by setting a voltage, it is preferred to set the desired current with a beforehand adjusted current controller. Whereas the output voltage of the current controller is used in the calculation.

3.5 Transient Inductance

In the rotor flux oriented control, the transient inductance is at least required to tune the current controller. This makes the σL_S an important parameter in the control system. For an optimal and stable control, the CC parameters need to be set according to σL_S. Considering the IM step response, an underestimated transient inductance leads to a longer settling time and a higher overshoot. Hence reducing the dynamic performance of the system. On the other hand, an overestimated value, could render the system unstable. [11]

3.5.1 Transient Methods

Voltage Pulse

The voltage pulse method is one of the first self-commissioning techniques. [34] In principle the test consists of applying single axis pulses to the IM and measuring the elapsed time between preset values of the current.[18, 11, 31] Figure 3.3 shows the test injection and response. First a positive voltage pulse is applied till the rated current is reached. After sufficient time the voltage pulse is reversed.
Under this condition the flux change is almost zero due to the short pulse interval. Hence, the magnetizing inductance can be neglected and the stator voltage can be expressed as:

$$u_S = (R_S + R'_R)i_S + \sigma L_S \frac{di_S}{dt} \tag{3.12}$$

The transient inductance can be calculated using only the first pulse. According to [34] though using the second current slope increases the accuracy of the transient test. Based on the assumption that the voltage drops over the resistors are small compared to the applied voltage, an additional simplification can be made. Thereby dropping the stator and rotor resistance from equation 3.12. Using only the first current slope, σL_S is then computed using the final current value at t1 the voltage and the time instant the rated current is reached, t1.

$$\sigma L_S = U_{S0} \frac{t1}{I_{S0}(t1)} \tag{3.13}$$

For the second current slope, the time difference (t3-t2) and the current difference between the start and the end of the second pulse is utilized.

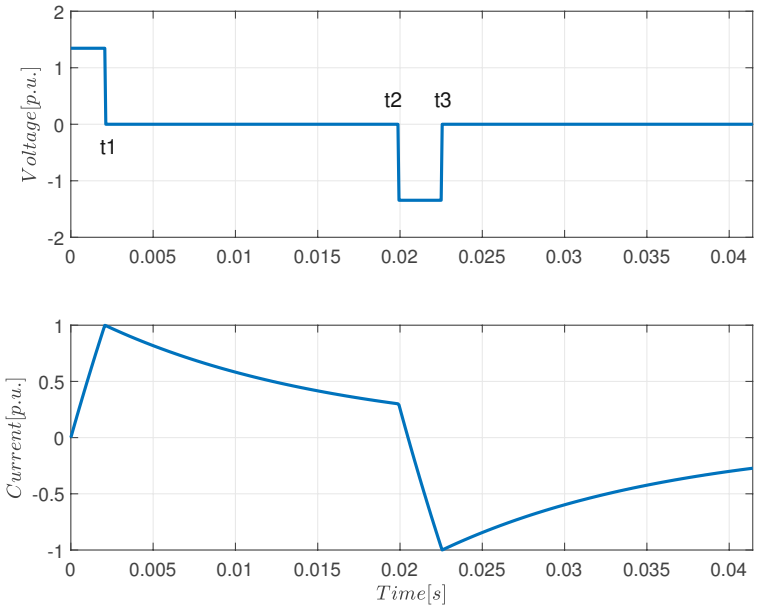

Figure 3.3: In the top figure, the single axis voltage is shown. The bottom figure shows the stator current response of the machine.

$$\sigma L_S = U_{S0} \frac{\Delta t}{\Delta I_{S0}} = U_{S0} \frac{t3 - t2}{I_{S0}(t2) - I_{S0}(t3)} \tag{3.14}$$

The height of the applied voltage pulse determines the slope of the current. A disadvantage of this test is due to the limited sampling frequency of the inverter. When the transient inductance of the IM is very low, the current slope can be to fast for the inverter to stop the pulse at the rated current. Therefore, running the risk of an over-current that could harm the machine. Reducing the applied voltage with PWM however, increases the error produced by the voltage drops over R_S and R'_R. The extent of this disadvantage is best explained using an example. Considering a single axis excitation with $\vartheta = 0$. The inverter sampling frequency f_s is 16kHz and the DC-Link voltage is 560V. Without PWM and $\vartheta = 0$, the voltage applied to phase u is $2/3U_{DClink}$. Therefore t1 is reached after:

$$t1 = \sigma L_S \frac{\sqrt{2} I_N}{2/3 \cdot U_{DC-Link}} \tag{3.15}$$

The number of current samples till the voltage pulse should end can then be calculated with:

$$Samples = rounddown(t1 \cdot f_s) \tag{3.16}$$

To verify the applicability of this method the possible number of samples till t1 was calculated for the known parameters of several hundred different induction motors. Table 3.2 shows the result of this evaluation till a possible number of 20 samples. For 27,2% of the motors, 20 samples or more can be taken till the rated current is reached. Less than 3 samples are possible for 3,1%. Apart from possible harm to the winding

Minimum number of samples till the rated current is reached	Percentage of Motors
3	96,9%
5	80,2%
10	64,5%
15	42%
20	27,4%

Table 3.2: Minimum number of samples that can be recorded till the rated current is reached when a single axis DC voltage pulse is applied. The right column shows the percentage of the investigated motors where at least 3,5,10,15 or 20 samples can be taken. $U_{S0} = U_{DC-Link}, \vartheta = 0$

due to over-current, the low sample number decreases the accuracy of this test.

To increase the robustness of this test, [11] proposes to inject a fast controlled current ramp. Whereas the ramp should be fast enough to allow neglecting the magnetizing inductance but slow enough to be able to record several samples. A disadvantage thereby is that the current controller needs to be initialized beforehand. This can be done by setting an initial value of KP and KI=0. Then the step response is measured and KP is iteratively adjusted to get the desired overshoot (e.g. 10%). When the desired KP is obtained, KI is calculated with the desired time constant TN (e.g. 2 ms).

$$KI = \frac{KP}{TN}$$

Current Steps

A disadvantage of the voltage pulse test is that saturation effects are not considered. In order to get the saturation characteristics of σL_S a different approach is proposed here that also utilizes the current controller. While it is required to initialize the CC beforehand with e.g. the method proposed above, the test provides a safer option for self commissioning. Here, a sequence of current steps is applied to the IM. This sequence is shown in figure 3.4. σL_S is then calculated for each step that represents a saturation sate of the motor.

The transient inductance could be obtained using a curve fit. However, the criterion on low computational power demands a different approach. This approach is based on solving a simplified state space model of the IM and the PI current controller. As the fast response of the IM is required, only R_S and σL_S are considered in the IM. Leading to the transfer function:

$$G_M = \frac{1}{s\sigma L_S + R_S} \tag{3.17}$$

Instead of the PI controller only a proportional segment(KP) is taken into account. It is assumed that neglecting the effect of KI in the calculations does not pose a significant error. Taking KI into account would significantly increase the complexity of the closed loop transfer function which then requires an approximation method for

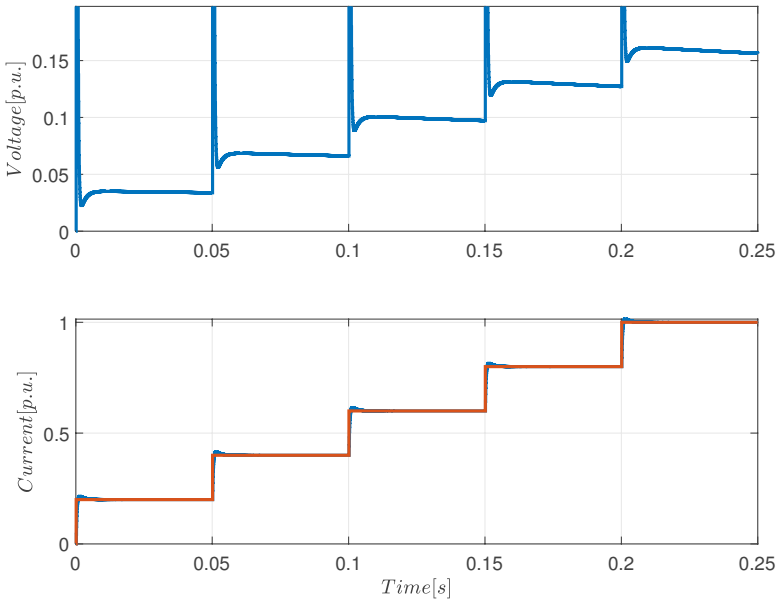

Figure 3.4: Injection sequence of the current steps test.

solving. Therefore leading to the closed loop transfer function:

$$G = \frac{KP}{\sigma L_S(s + \frac{R_S+KP}{\sigma L_S})} \tag{3.18}$$

Using the impulse response:

$$H = \frac{G}{s} \cdot K \tag{3.19}$$

where K is the step height, the step response is obtained as:

$$h(t) = K\frac{KP}{R_S + KP} \cdot \left(1 - e^{\frac{R_S + KP}{\sigma L_S} \cdot t}\right) \tag{3.20}$$

Using a specific point (t=t_1) of the step response and rearranging 3.20, the transient inductance can be calculated.

$$\sigma L_S = \frac{1}{-\ln\left(1 - \frac{\frac{h(t_1)}{K}(R_S+KP)}{KP}\right)} \cdot (R_S + KP) \cdot t_1 \tag{3.21}$$

Additionally, if $KP >> R_S$, R_S becomes also negligible. The difficulty of using this method is to set the current controller accordingly and to choose the time instant t_1 for sampling. t_1 is obtained by searching for the moment, the response reaches a certain amount of the step height K. Hence this factor is introduced as $h(t_1)/K = \alpha$. Where, $0 < \alpha < 1$.

3.5.2 High Frequency Single Phase Excitation

This method identifies the inductance by means of a high frequency single phase test.[21, 34, 22, 27, 35] Introducing, the total impedance of the inverse Γ equivalent circuit 2.4,

$$Z = R_S + j\omega\sigma L_S + \frac{j\omega(1-\sigma)L_S \cdot R'_R}{j\omega(1-\sigma)L_S + R'_R} \tag{3.22}$$

where $\omega = 2\pi f$, with f being the frequency of the injected signal. The last term of 3.22 converges to R'_R as the frequency increases. Therefore, for high frequencies the impedance reduces to:

$$Z = R_S + R'_R + j\omega\sigma L_S \tag{3.23}$$

Using the imaginary part of the impedance, the transient inductance can be estimated. The rotor resistance could also be estimated with the real part and knowledge of R_S. This however is not advisable as the resistance could increase at very high frequencies due to skin and proximity effects. [21] For a high enough injection frequency the imaginary part yields the value of σL_S.

$$\sigma L_S = \frac{Im\{Z\}}{\omega} = \frac{1}{\omega}\frac{U_{S1}}{I_{S1}} \cdot sin(\varphi) \tag{3.24}$$

To compute σL_S, the amplitude of both current and voltage needs to be known. Further, the phase shift between those two is also required. As the injection frequency is known, obtaining those values can be accomplished using e.g. the Goertzel algorithm or resonant filters. To reduce the computational effort, the frequency could also be chosen high enough to consider, $sin(\varphi) = 1$. This is the case when:

$$f >> \frac{R_S + R'_R}{2\pi\sigma L_S} \tag{3.25}$$

As implied by 3.23 only the AC component of the single phase signal is used to calculate the transient inductance. However, a DC component can be added to saturate the IM. In addition, superimposing a DC component has the advantage of not having to deal with inverter dead time effects. Applying a suitable injection frequency is of great importance. [21] proposes 300Hz for a 50Hz IM whereas [27] uses 200Hz. On contrast, in [34] a 30Hz signal is deemed to already provide accurate results. For practical reasons, multiples of the power grids frequency(50Hz or 60Hz) should be avoided. The DC-link voltage contains harmonics of this frequency which will also be visible in the inverter output voltage. Therefore the determination of AC component suffers from these multiples.

3.6 Magnetizing Inductance

As stated before the parameters of the inverse-Γ EC are in focus. Therefore when speaking of the magnetizing inductance, $(1-\sigma) \cdot L_S$ is meant. When $(1-\sigma) \cdot L_S$ and σL_S are identified, σ and L_S can be calculated directly. Further L_M and L_R are obtained with these parameters. In the mentioned flux oriented control, L_S is needed

for the field weakening. L_R or $(1 - \sigma) \cdot L_S$ can be used to compute the rotor time constant τ_R. Section 3.8 introduces methods to obtain τ_R directly. Hence, the main goal is to identify L_S. The value of the magnetizing inductance varies with the magnetizing current since the rotor core gets saturated. At higher currents the inductance decreases from its unsaturated value.

3.6.1 Low Frequency Single Phase Excitation

The first method aims to identify $(1-\sigma)\cdot L_S$ by means of a low frequency single phase test. [22, 32, 20, 23] Similar to 3.5.2 a sinusoidal single phase current is injected. The main difference is that the injection frequency is now very low. Equation 3.22 can be rewritten by separating its real and imaginary part. These are also computed with the measured values of U_{S1}, I_{S1} and their phase shift.

$$R = real(Z) = R_S + \frac{R'_R(\omega(1-\sigma)L_S)^2}{R'^2_R + (\omega(1-\sigma)L_S)^2} = \frac{U_{S1}}{I_{S1}} cos(\varphi) \tag{3.26}$$

$$X = imag(Z) = \omega\sigma L_S + \omega\frac{R'^2_R(\omega(1-\sigma)L_S)}{R'^2_R + (\omega(1-\sigma)L_S)^2} = \frac{U_{S1}}{I_{S1}} sin(\varphi) \tag{3.27}$$

Solving 3.26 and 3.27 leads to the following expression for the magnetizing inductance.

$$(1-\sigma)L_S = \frac{(R-R_S)^2 + (X-\omega\sigma L_S)^2}{\omega(X-\omega\sigma L_S)} \tag{3.28}$$

[23] proposes to chose the injection frequency according to:

$$\omega <= \frac{1}{8}\frac{R'_R}{\sigma L_S} \tag{3.29}$$

where R'_R and σL_S are estimated using the nameplate data. At lower frequencies, computation of the magnetizing inductance becomes insensitive to σL_S errors. To obtain L_S at different saturations, [20] varies the amplitude whereas in [32] a superimposed DC current at different levels is used.

3.6.2 Transient Test

The second method to identify the magnetizing inductance of the inverse Γ circuit, introduced here is a DC-decay test. The test consists of two steps. [35, 21] In the first step, a DC current I_{DC} is injected into the IM. The current value sets the operating point. At t=0, the circuit is in steady state DC condition. The stator flux can be obtained by rearranging and integrating the stator voltage equation.

$$\int_0^t (u_S - R_S i_s)dt = \Psi_S(t) - \Psi_S(0) \tag{3.30}$$

where $\Psi_S(0)$ and $\Psi_S(t)$ are the stator flux in DC steady state and at the time instant t. In the second step a null voltage vector is applied and both the current and the flux converge to zero $(u_S(t=0)=0)$, reducing the equation to,

$$\lim_{t\to\infty}\int_0^t (u_S - R_S i_s)dt = -\Psi_S(0) \tag{3.31}$$

At t=0, the stator flux is determined by L_S and the current value. Therefore the stator inductance can be calculated using

$$L_S = -\frac{1}{I_{DC}} \lim_{t\to\infty} \int_0^t (u_S - R_S i_s) dt = \frac{\Psi_S(0)}{I_{DC}} \tag{3.32}$$

In practice the integration can be continued till the measured current falls below the detectable sensibility of the AD converter. The biggest disadvantage of this method is that the characteristics of the inverter switches need to be known. During the integration, u_S is set to null in the inverter. Therefore either the upper or the lower 3 switches are in on state. The circuit is not perfectly short circuited due to voltage drops over the IGBTs and diodes. These voltage drops are represented by u_S in the equation. As the inverter cannot measure the voltage u_S needs to be reconstructed from the current and the characteristics of the semiconductors.

3.7 Rotor Resistance

The rotor resistance is the most sensitive parameter of a squirrel cage IM. Due to the thermal drift produced by rotor currents in the shortened rotor bars R'_R varies with the temperature. As the temperature heavily depends on the operation, lot of research is directed to online tracking of the resistance. Offline estimation does serve as a starting point but as soon as the machine is loaded, the rotor currents will generate heat and render the standstill estimation erroneous. However, if the machine possesses a temperature sensor, the resistance can be adjusted using the rotor resistances temperature coefficient. In contrast to R_S, R'_R cannot be measured with a simple DC test, since the rotor of a squirrel cage IM is electrically inaccessible. The rotor resistance is required for the computation of τ_R, if not obtained directly as in 3.8.

3.7.1 Low Frequency Single Phase Excitation

Using the same supply as in 3.6.1, the rotor resistance can also be identified. In [21, 27, 31, 20, 33] a low frequency single phase current with a DC component is applied. Frequencies higher than the nominal slip speed are not meaningful because they do not fall under the normal working conditions of a vector-controlled IM drive. [21] [31] suggest the frequency ω to be determined using the following condition:

$$\frac{R_R + j\omega L_{\sigma R}}{j\omega L_M} < 0.05 \tag{3.33}$$

where the parameters are estimated using the nameplate. Rearranging 3.26 and 3.27 R'_R is computed with:

$$R'_R = \frac{(R - R_S)^2 + (X - \omega\sigma L_S)^2}{R - R_S} \tag{3.34}$$

σL_S and R_S need to be identified before and influence the accuracy of R'_R. Whereas the σL_S used here should be identified at the same saturation level where the R'_R-test is conducted.

3.8 Rotor Time Constant

The rotor time constant τ_R is an important parameter in field oriented control systems. Estimation of the flux inside the machine requires accurate knowledge of τ_R. Using the following equations the rotor time constant can be expressed with the T or Inverse-γ equivalent circuit parameters.

$$\tau_R = \frac{L_R}{R_R} \; or \; \tau_R = \frac{(1-\sigma) \cdot L_S}{R'_R} \tag{3.35}$$

Due to its direct dependency on the rotor resistance, magnetizing and leakage inductance the parameter itself also changes with temperature and saturation. The proposed standstill identification methods however provide an estimate at a specific operating point. For accurate determination of the rotor time constant over the whole range of operation, online tracking would be required. Since the determination of the rotor resistance can be quite hard, the following two methods described below aim to identify τ_R directly without using the equation above.

3.8.1 Single Phase Current Injection Strategy

In the first method, a controlled single axis current, with the frequency ω and amplitude $\hat{I}$ is injected into the IM until the machine reaches a steady state. At the precise time instant, where the sinusoidal input equals the desired magnetizing current, the reference current is switched to DC (I_{DC}). [11] [18] [36] This sequence is illustrated for one phase current in figure 3.5.

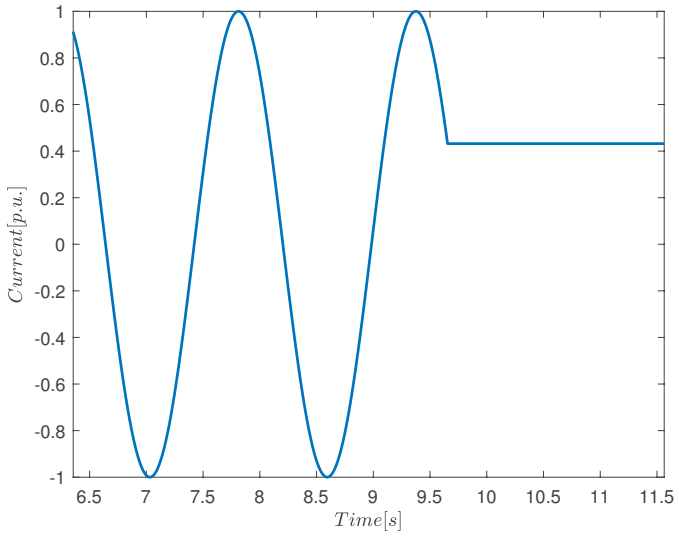

Figure 3.5: This figure shows the reference current of one phase for the single phase current injection strategy

If at this time instant the actual magnetizing current i_m in the machine does not equal the desired one, a voltage transient can be observed at the stator terminals. The

occurrence of this transient can best be explained with the equivalent circuit 2.4 and the fact that the current through the magnetizing branch cannot be changed instantly. Three cases must be considered which are displayed in figure 3.6 When the i_m is lower the set DC value (a), the additional current will flow through the rotor resistance resulting in a positive voltage transient. In (c) the magnetizing current is to high and the excess energy stored in the magnetizing branch manifests in a current through the rotor resistance. This time though in the opposite direction as in (a) which creates a negative transient. (b) shows the case where i_m equals the DC value at the switching instant. As the magnetizing inductance already holds this current the voltage transient disappears and current controller output voltage equals only the voltage drop over R_S and the IGBTs. The DC current value of (b) also equals the amplitude of i_m before the switching instant. At this point τ_R can be calculated using:

$$\tau_R = \frac{1}{\omega} \cdot \frac{\sqrt{\hat{I}^2 - I_{DC}^2}}{I_{DC}} \tag{3.36}$$

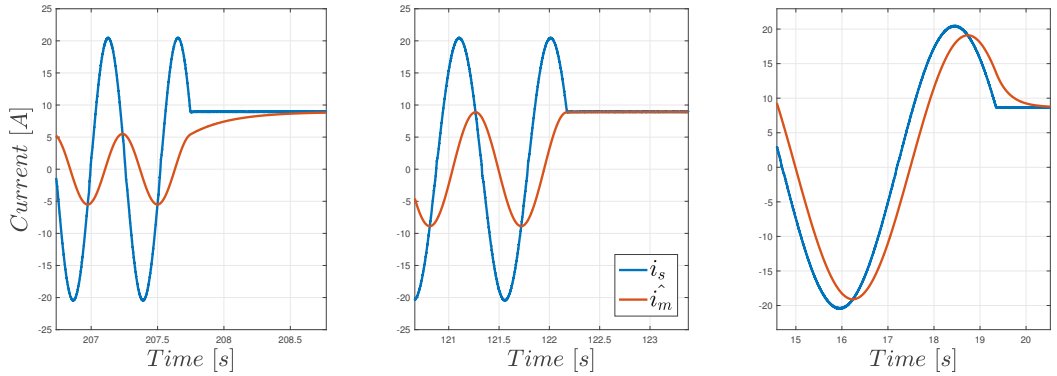

(a) (b) (c)

Figure 3.6: This figure shows the reference current(blue) and the estimated magnetizing current(red). Whereas the single phase amplitude and the DC value are kept the same, the frequency is varies from a-c. In a the frequency is chosen to high, in b just right and in c to low.

Normally a rotor flux oriented control system operates at a fixed operating flux or magnetizing current. The magnetizing inductance as well as the rotor time constant depend on the value of i_m. Therefore it is desirable to conduct the tests for constant I_{DC} level which produces the desired flux inside the machine. By varying the frequency or the amplitude of the sine input, the value of i_m at the switching instant can be influenced. In summary the goal is to find an amplitude/frequency pair where the voltage transient is below a detectable value.

[11] suggests an iterative approach where one value is kept constant and the other is increased or decreased depending on the sign of the voltage transient. As the wanted frequency is in the range of the slip frequency, a different approach would be to take several measurements below and above ω_{slip}. Then calculate the τ_R estimate for each

measurement and use interpolation to find the point where the transient is supposedly zero.

To obtain the transient the output of the current controller can be used. A big advantage is that the non linearities of the inverter do not reduce the accuracy because only the relative voltage difference is used. In [18] the voltage difference Δu between the beginning and the end of the transient is use as the iteration criterium. This is improved by the idea to calculate the voltage-time area ΔA in [11]. Using ΔA instead of Δu the method becomes less afflicted by noise. Figure 3.7 shows the voltage after the switching instant. ΔA is calculated with $\Delta A = A_1 - A_2$.

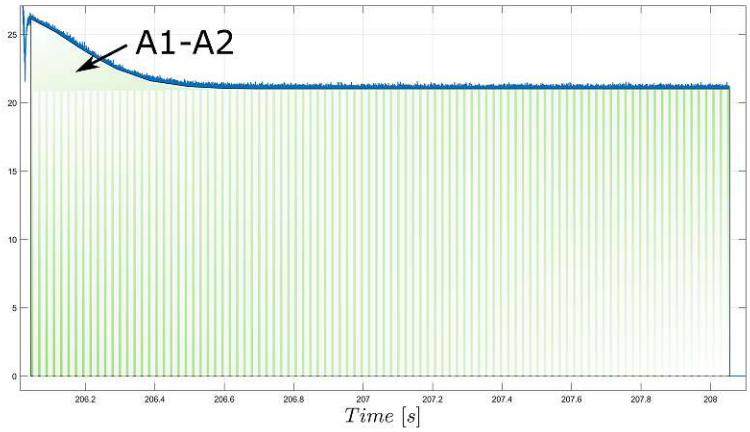

Figure 3.7: This figure shows the voltage transient after switching to DC. The green area represents A_1. The white striped area is A_2. The difference between those is $\Delta A = A_1 - A_2$

3.8.2 Flux Observer based Strategy

The second rotor time constant identification strategy uses a different excitation of the IM. This method requires an initial τ_R estimate from the nameplate data and uses a flux observer (3.8) to estimate the magnetizing current. [37]

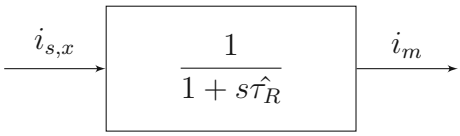

Figure 3.8: This figure shows a current based flux observer. With the estimate of τ_R ($\hat{\tau_R}$) the magnetizing current is calculated. i_m multiplied with the magnetizing inductance $L_s(1-\sigma)$ would further provide an estimate of the rotor flux.

As depicted in figure 3.9, first a controlled DC current i_s is applied to the motor. After sufficient time has passed till the i_m equals the stator current, the reference is switched to its negative DC value. When the estimated magnetizing current $\hat{i_m}$ then equals the

rated magnetizing current I_{MN} the reference is switched to $-I_{MN}$. If the estimate $\hat{i_m}$ is right, the voltage seen at the current controller output equals the voltage drop over R_S and the IGBTs. Due to the same reason described in 3.8.1, a false estimate results in a voltage transient seen at the stator terminals.

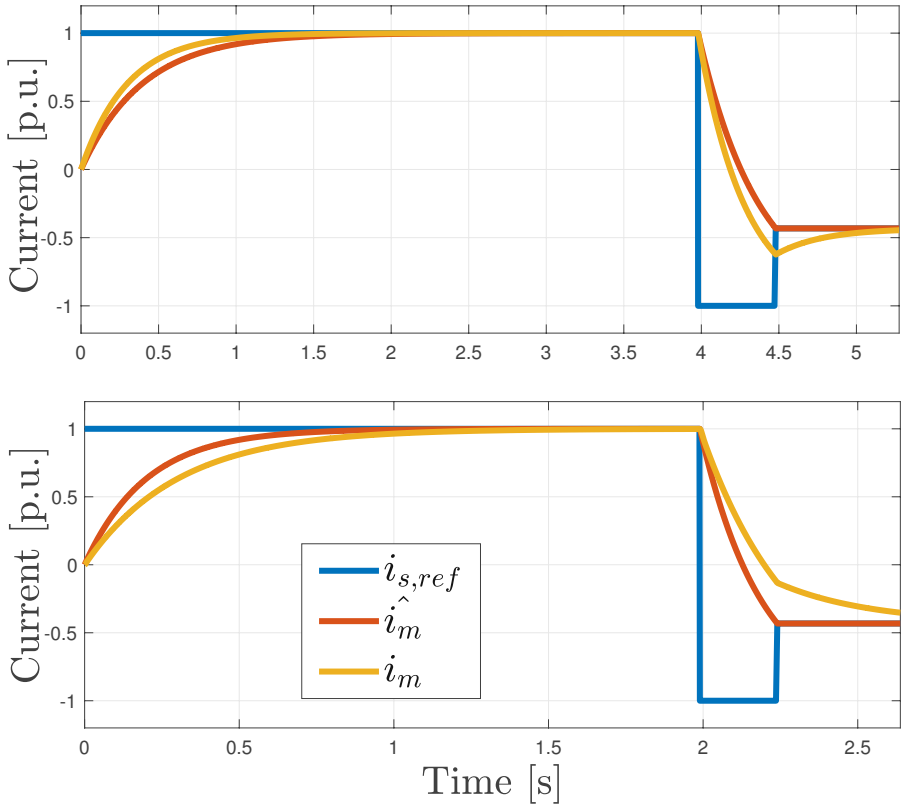

Figure 3.9: In this figure, the injection sequence for the τ_R estimation is shown with $i_{s,ref}$. $\hat{i_m}$ is the estimated magnetizing current and i_m the IMs actual value. The curves are obtained in simulink. The upper plot shows case for $\hat{\tau_R} < \tau_R$ whereas in the lower plot $\hat{\tau_R} > \tau_R$

Figure 3.10 shows this transient for two $\hat{\tau_R}$. A positive transient can be observed when, $\hat{\tau_R} > \tau_R$ or $|\hat{i_m}| < |i_m|$ at the third switching instant. The negative one is seen when, $\hat{\tau_R} < \tau_R$ or $|\hat{i_m}| > |i_m|$ at the third switching instant. In [11] an iterative approach is used to minimize the voltage transient by adjusting $\hat{\tau_R}$ in each iteration. When the voltage transient is below a detectable level, the estimate is right. Equally to 3.8.1 the area below the voltage transient ΔA is used as the iteration criterium.

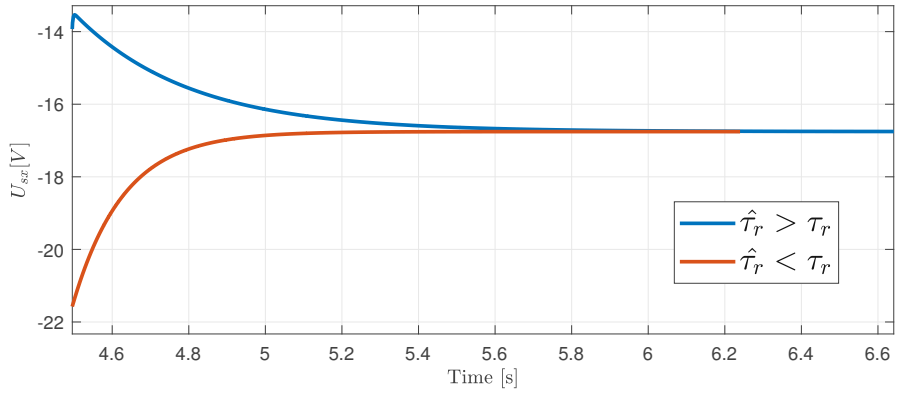

Figure 3.10: The voltage transient after the third switching instant is shown here for two different $\hat{\tau_R}$. It can be seen that in both cases the voltage converges to the same final value caused by R_S and the inverter switches. This plot was recorded in simulink.

CHAPTER 4

Results

To evaluate the methods described above, they are first tested in a Matlab/SIMULINK model which is briefly described in 4.1. Then tests were performed on an IM using a power inverter. The setup used is mentioned in 4.2. The results using the simulation and the measurements are then shown for each method.

4.1 Simulation Environment

Before testing the methods in a real environment, a simulation was used to verify their integrity. Therefore an IM model was created in Matlab/Simulink. The simulations were made with the simulink model shown in figure 4.1. The model is based on [38] and uses the space phasor equations of the inverse-Γ equivalent circuit. In this IM model, the stator voltage and the load torque are the inputs. Outputs are the produced torque, the speed and the resulting stator current phasor. As all the test are done at standstill, the produced torque is set the same as the load torque. To predict the behaviour of the IM, later used of testing, the same motor parameters were used in the model. All IM parameters are considered as constant in the simulation as no data was available to model the saturation characteristics, the influence of the temperature, or frequency related effects. Hence the values obtained in simulation are not directly comparable to those of the real measurements. But the simulation provides valuable information about injection frequencies etc.. Furthermore, the sampling frequency is fixed to 16kHz which is the same used by the inverter in the experimental setup.

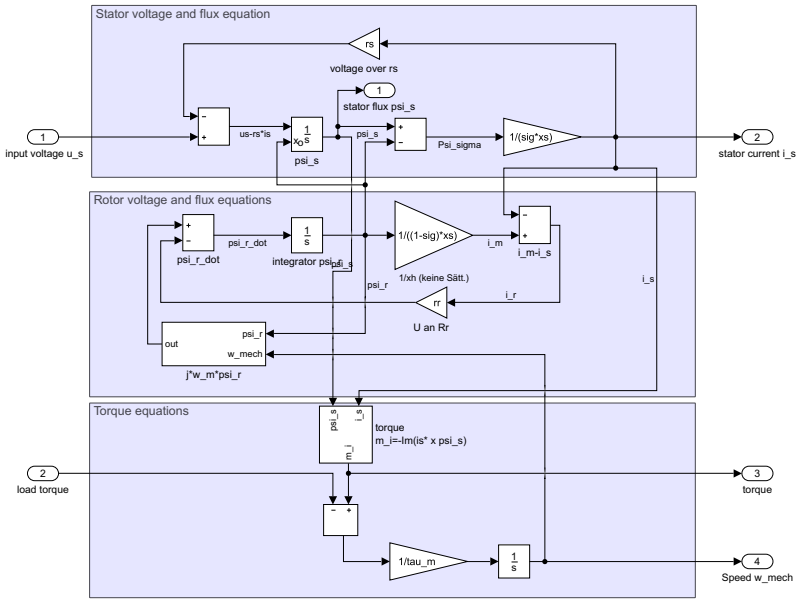

Figure 4.1: Simulink model of an induction machine

4.2 Experimental Setup

To verify the applicability of the proposed identification schemes, the methods were tested on a squirrel cage induction machine. Figure 4.2 illustrates the setup.

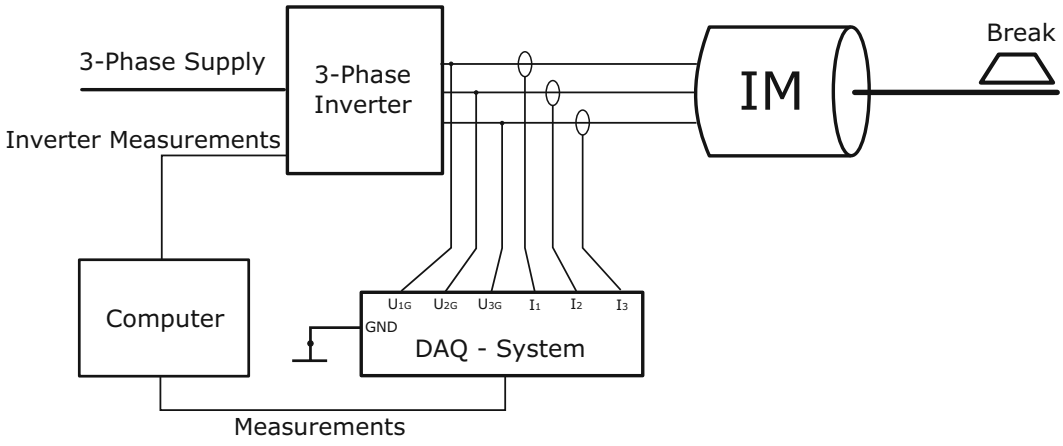

Figure 4.2: Scheme of the Experimental Setup

All test signals are created with the inverter which supplies the induction motor. Measurements are obtained from the inverter and an additional digital oscilloscope. The Data is then stored on a computer and evaluated in Matlab. No load is connected to the motor but the rotor can be blocked with an electromagnetic break. This break is able to withstand up to twice the motors nominal torque.

Power P_N	Voltage U_N	Current I_N	Frequency f_N	Power Factor
4,6kW	340V	12,5A	16Hz	0.87

Table 4.1: Nominal values of the tested induction motor.

Induction Motor The tests were performed on a 4,6kW squirrel cage induction motor with nominal values illustrated in table 4.1.

Inverter The inverter is capable of measuring two phase currents, the DC-link voltage $U_{DC-link}$, the temperature of the IM and the rotational speed. Additionally I_1 and I_2 are lowpass filtered before being stored. To acquire the phase voltages, the DC-link voltage and the PWM switching pulses are used. All measurements are recorded with 16kHz.

DAQ-System In order to study the influence of the inverter non linearities which renders the reconstructed voltage erroneous, a DAQ-System is used to measure the line currents and voltages. The DAQ-System is a custom Sirius module from Dewesoft. Via USB connection and the DewesoftX2 software the data gets stored for further processing in Matlab.

The phase to ground voltage(U_{1G}, U_{2G}, U_{3G}) is measured for each phase directly at the inverter output. By calculating the offset voltage U_0 and subtracting, the phase voltages U_1, U_2, U_3 are computed.

$$U_0 = \frac{1}{3}(U_{1G} + U_{2G} + U_{3G}) \tag{4.1}$$

$$U_1 = U_{1G} - U_0 \tag{4.2}$$

$$U_2 = U_{2G} - U_0 \tag{4.3}$$

$$U_3 = U_{3G} - U_0 \tag{4.4}$$

The line currents (I_1, I_2, I_3) are measured with DS-CLAMP-150DC current clamps directly at the inverter output terminals. To eliminate the influence of any unwanted capacitive currents, the same calculation as for the voltages, is applied to the currents. All DAQ measurements are recorded at a 1MHz sample frequency. Additionally the data is low pass filtered with a 100kHz 5th order Bessel filter to avoid anti aliasing.

4.3 Standard IEEE Test

In addition to the standstill identification methods, the standard locked rotor and no-load test was performed in order to get comparable values. The calculations were made with the equations proposed in the IEEE standard [9]. As no additional power supply was available the tests were conducted using the inverter and the DAQ-System measurements. Although it would be more accurate to use a real sinusoidal supply, [39] states that using an inverter for the standard test is also valid.

1. Transient inductance σL_S
2. Stator resistance R_S
3. Magnetizing inductance $(1-\sigma)L_S$
4. Rotor time constant τ_R and/or rotor resistance R_R

Figure 4.3: Proposed identification work flow.

4.4 Self commissioning procedure

The equivalent circuit parameters could be identified in any given order. However some considerations should be made. Some methods require an operating current controller for application. Therefore, the parameters which are used for the CC tuning should be identified first. Optimum gains for the PI current controller are set using the transient inductance and the stator resistance. [40] In some cases the stator resistance is neglected due to its small value. However, the stator resistance is necessary for the calculation of the magnetizing inductance. When the parameters are identified separately a possible work flow is depicted in 4.3.

4.5 Stator Resistance

As mentioned in section 3.4 only the DC-test is evaluated. When a step current is applied, a voltage transient appears at the current controller outputs. This can be seen in the lower plot of figure 3.2. The phenomena is explained by looking at the equivalent circuit. After the step is applied, the current first flows through the rotor branch as the magnetizing inductance does not allow rapid current change. For the calculation of the stator resistance the steady state of the DC-injection is required. Hence, the data needs to be obtained after the transient disappears. Nevertheless it should be kept in mind that applying the DC current for a too long timespan can heat the stator windings and falsify the results. Additionally the current steps should be high enough so that the inverter non linearities do not effect the results.

Simulation

In Simulink, the method was tested for various different step heights. Figure 4.4 shows representative results of two different inputs in comparison to the time required to take the measurements. The red plot shows the result of the R_S calculation when at first 0.8 I_N and then I_N is applied to the IM. Blue is obtained with the first step being $0.5I_N$ and the second I_N. The difference in the error is the product of the before mentioned voltage transient which is higher for bigger current steps. Therefore, when applying steps with different heights, the required waiting time differs. Using the same step height for both steps and sampling the data after the same time minimizes the influence of an error produced with sampling too soon. Varying the total step height but keeping the value of the first step at half the second step also results in the blue curve from figure 4.4. Nevertheless, it should be mentioned here that the voltage transient in a real IM will differ in height also due to saturation effects.

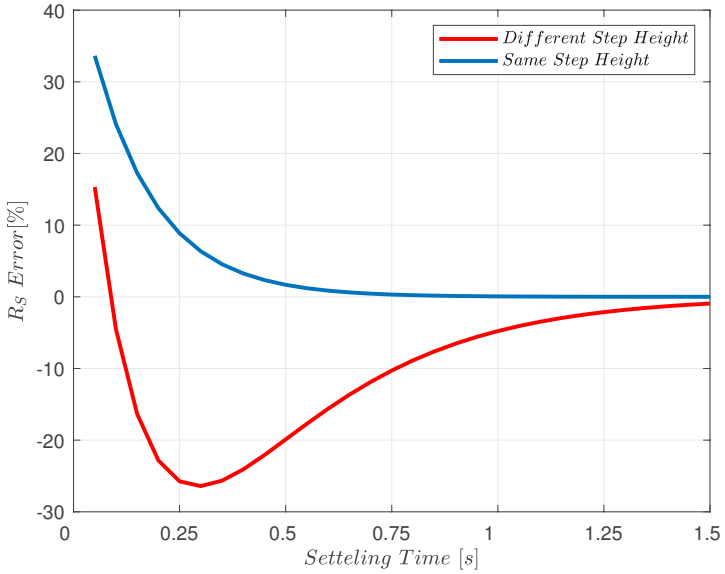

Figure 4.4: This figures y-axis shows the R_s error in percent. The x-axis represents the time waited after each step to acquire the measurements for the calculation of R_S. The red line is obtained with the first step being 0.8 I_N and the second 0.2 I_N. For the blue line the 2 steps possess same height 0.5 I_N.

The required waiting time depends on the rotor time constant. τ_R of the IM under investigation is 300ms. Using the nameplate data estimates usually results in a lower $\hat{\tau_R}$. In this motors case $\hat{\tau_R}$ is 32% less with the value being $\hat{\tau_R} = 205.5ms$. Hence, it is recommended here to apply two steps with the same height, and to record the voltage and current after $4 - 5 \cdot \hat{\tau_R}$ where the error is below 0.5%.

Experimental Environment

The whole test consists of 3 R_S measurements at different space angles ϑ. As illustrated in figure 4.5, choosing the space angle as, $30°, 90°$ and $150°$ only 2 phases are conducting while the third is controlled to zero. Since the voltages and the currents now also inhibit noise, their average over a short time is used. R_S is computed using 3.11 in each 2-step sequence and then the mean value is taken. The value is computed with the inverter currents and the current controller output voltage on the one hand and using the DAQ measurements on the other.
Figure 4.6 shows the difference between the real voltage applied to the machine and the voltage set by the inverter. As already mentioned the difference mainly comes from the voltage drops over the inverter switches.
By varying the step heights, various measurements were taken. With the DAQ-system measurements, an R_S value of 1.9031Ω could be calculated.
Using the inverter, valid results could be achieved using the step heights of $0.5 \cdot \hat{I_N}$ and $\hat{I_N}$. R_S was computed as 1.9928Ω which equals an error of 4.88%. Lowering the current steps results in differing inverter non-linearities. Applying a current that is too high,

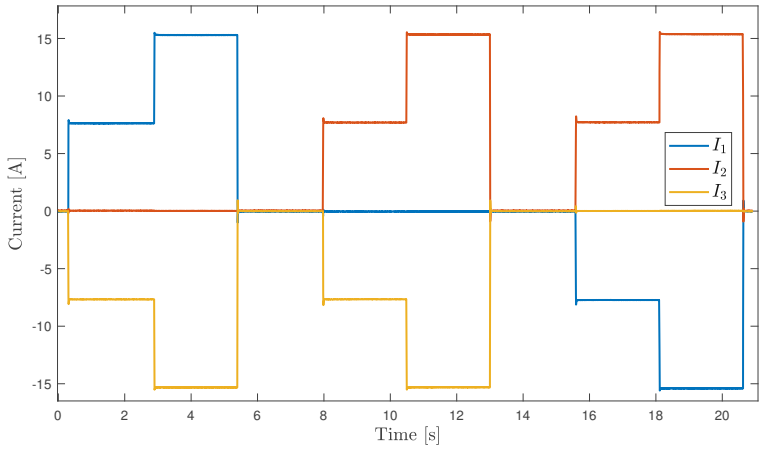

Figure 4.5: Three phase currents during the stator resistance identification.

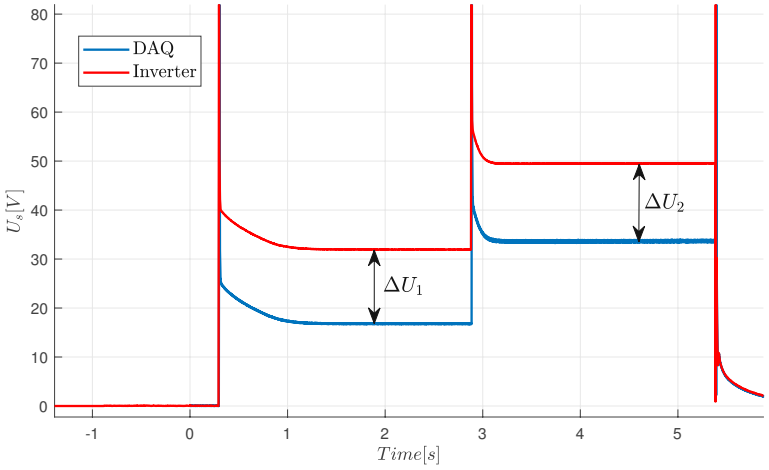

Figure 4.6: Real voltage(red) vs. the voltage seen at the current controller output(blue). $\Delta U_1 = 15.1V$,$\Delta U_2 = 15.8V$

causes warming of the coils which also renders the result erroneous. In comparison to the simulation, the required waiting time, differs significantly for the two steps. This can be seen in figure 4.6. During the first current step, it takes much longer for the voltage to reach its steady state value. The cause of this, is the saturation of the magnetizing inductance which influences the rotor time constant. Thus, the assumption that using the same step height for the first and the second step yields better results, is not valid. Looking again at figure 4.6 it can be seen that the ΔU between the real voltage and the inverter voltage differs in both steps. Caused by the IGBT voltage drops, this deviation $\Delta U_2 - \Delta U_2 = 0.7V$ results in the above presented error. In order to reduce the influence of the IGBTs, the height of the first step was increased. The measurement was repeated by first applying $0.8 \cdot \hat{I_N}$ and then $\hat{I_N}$. Using this input, R_S was computed as 1.9531Ω which equals an error of 2.79%. Thus reducing the error by over 2%. The measurements have also shown that $5 \cdot \hat{\tau_R}$ is a sufficient waiting time at the proposed current levels.

4.6 Transient Inductance

4.6.1 Transient Methods

The transient methods were tested with the simulation and then on the mentioned IM. First, the approach with the positive and then negative voltage pulse is evaluated and secondly, the alternative approach using current controlled steps.

Voltage Pulse

By applying a voltage PWM signal to the IM and stepwise changing the pulse duration, the mean height of the voltage can be controlled. To evaluate the influence of the height of the pulse, the simulation was carried out for for a PWM pulse of 0.5-1 which equals a voltage of $1/3 \cdot U_{DC-Link}$ to $2/3 \cdot U_{DC-Link}$ on phase 1. The transient inductance is computed with 3.13 and 3.14 for each input. Figure 4.7 shows the calculated inductances and the real transient inductance. It can be seen that using the second pulse yields better results. This comes as no surprise and was already proposed by [34]. An overall trend towards the real inductance is also noticeable from the lower to the higher voltage pulses. Increasing the pulse leads to an increase of the current slope and therefore decreases the influence of the magnetizing inductance in the calculation. Anyway, using the second pulse, the σL_S error amounts to $11.4\% - 4.5\%$.

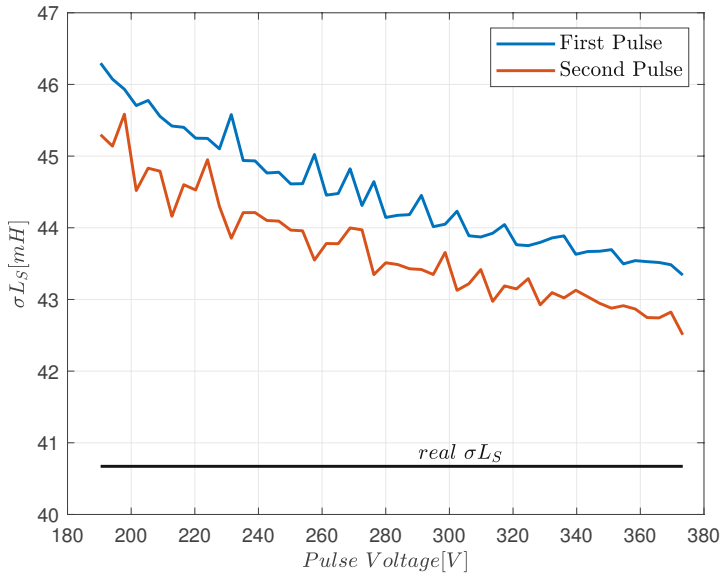

Figure 4.7: Estimated transient inductance for varying voltage pulses. The blue and red curves show the computed inductances using the first 3.13 and the second 3.14 pulse. In addition, the real transient inductance is plotted in black.

When performed within the test environment, the inverter dead time effects influence the current around the zero crossing points. This is shown in figure 4.8. The dead time negatively affects the calculation as it takes longer for the current to reach its rated value. Considering equation 3.14 a higher time difference results in a lower value of

σL_S. On the other hand, the reconstructed inverter voltage is higher than the measured one, leading to a higher inductance. With the DAQ measurements, the σL_S estimate is $27,3mH$. As expected the inverter measurements provide a slightly higher estimate of $29,2mH$.

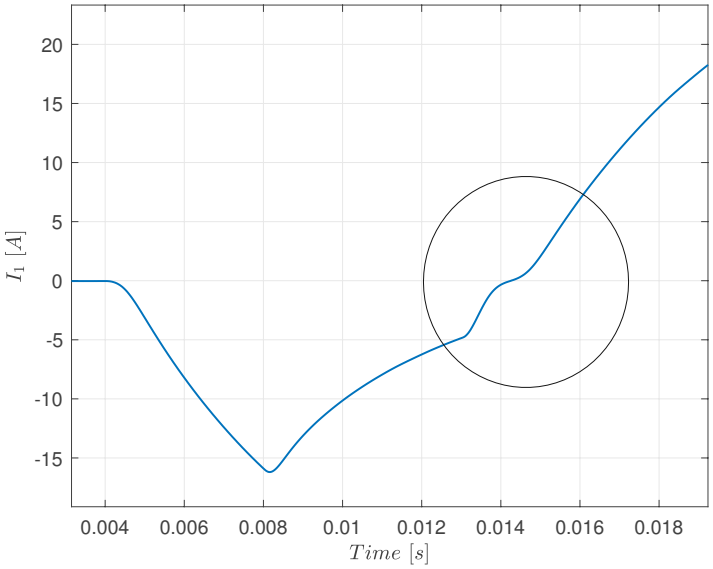

Figure 4.8: Current in phase 1 during the voltage pulse test recorded with the DAQ-system. The inverter dead time defect is highlighted with the circle.

Current Steps

Applying current steps instead of voltage pulses, poses less risk of over-currents for motors with a low reactance. As already mentioned in 3.5.1, tuning the current controller accordingly and choosing the right sample time instant, is essential for this method. Therefore, the effect of choosing different factors α and varying the CC parameters is researched in the simulation. As described in section 3.5.1, α defines the percentage of the current step at which the sample is taken for calculation.

Simulation In the simulation, the method was tested using a PI current controller. Figure 4.9 shows the result of the method where the integral element KI is set to zero. With a low value of α, the calculations become very accurate. At high α, the inductance becomes also higher. This is due to the influence of the magnetizing inductance at later sampling instances. As the current response is faster at a higher KP, the error also gets less. However, a faster response will also result in less sampling points. By setting KI of the CC with the method proposed at the end of section 3.5.1 and repeating the test, figure 4.10 was obtained. Here the inductance is mostly smaller due to the now wrong model of the system. However, with an increased proportional gain, the trend approaches the ones from figure 4.9. It can be seen that there is an optimum KP,KI pair that provides accurate results over the whole range of α. This optimum is represented

by the green curve. Considering R_S in equation 3.5.1 leads to overall better results. Even so, an optimum curve also exists without R_S.

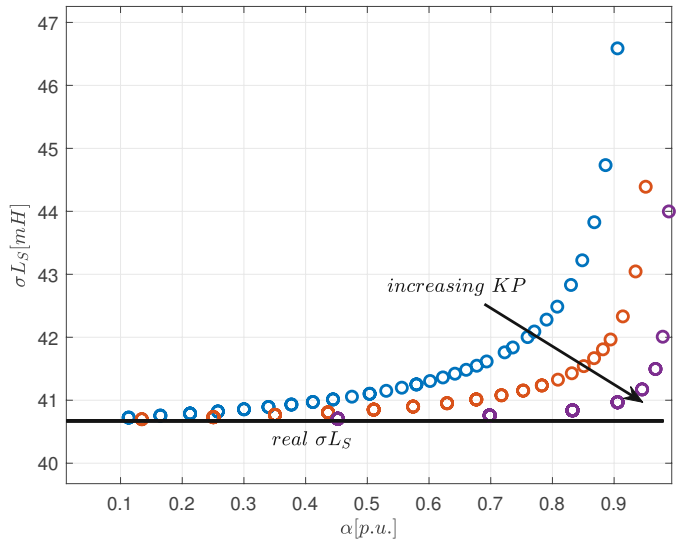

Figure 4.9: Transient inductance, at varying KP and α values with KI=0.

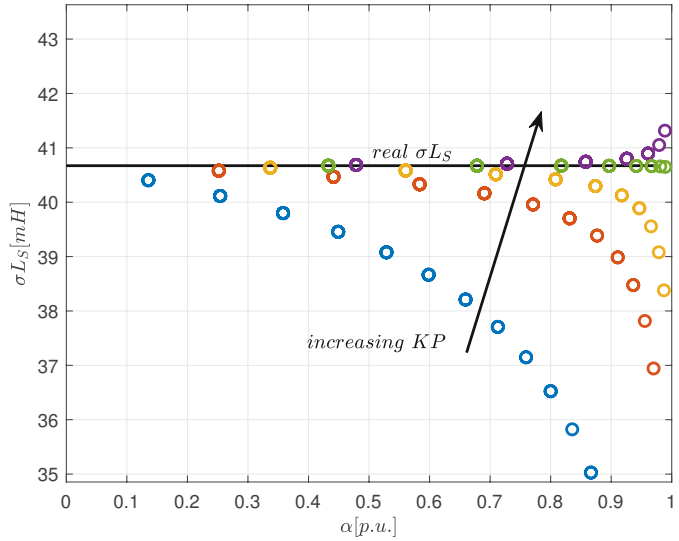

Figure 4.10: Transient inductance, at varying KP and α values with a constant KI=0,025.

By conducting various simulations, it was found that this optimum(neglecting R_S) can be reached with different KP,KI pairs. Thus, assuming KP is chosen high enough, KI can be calculated using the the following condition:

$$\frac{KP}{KI} = T_N = \frac{\sigma L_S}{R'_R + R_S} \tag{4.5}$$

This condition was found empirically, using the simulation. The calculated value of the transient inductance should then be accurate up to $\alpha = 0.9$. To increase the robustness of this method an iterative approach could be used. Thus, comparing the σL_S calculation at each sampling point from $\alpha = 0.2 - 0.8$. The nameplate data estimates can serve as an initial estimate of the KP/KI ratio. Then KI should be adjusted to minimize the deviation over α. If the error can not be minimized, KP is too low.

Experimental Environment The experimental setup used for testing did not allow for the integral element to be set to zero. Thus only a full PI controller could be tested. Since the voltage is not required in the calculations, no comparison to measurements with the DAQ-system are made. When the tests are conducted with the inverter exact knowledge of the time difference between the reference current and the measured current is required. In this case 2 controller cycles plus the time shift of the current filter equal $155\mu s$. Subtracting this value from the measured time leads to the actual value of T for equation 3.5.1. As the laboratory time was limited and the CC parameters could not be set freely, the optimum approach could not be tested. Since a not optimized PI controller is used, α needs to be set very low to acquire a reasonable estimate. With $\alpha = 0.2$ the saturation curve in figure 4.11 could be obtained. This coincides well with the curve obtained through the HF test.

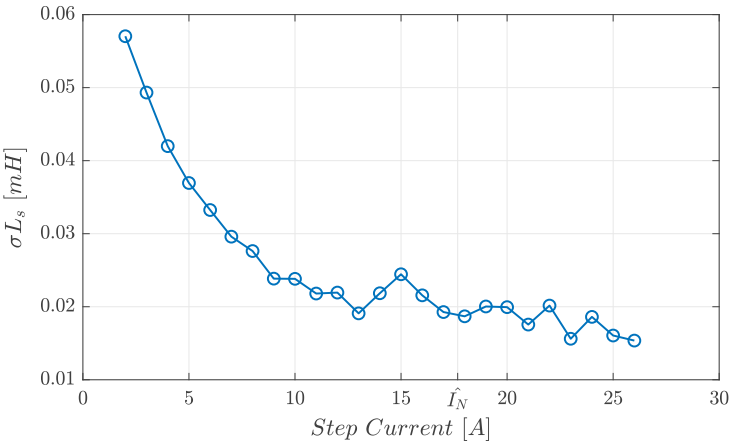

Figure 4.11: Saturation of the transient inductance obtained with controlled current steps.

4.6.2 High Frequency Single Phase Excitation

Simulation

The focus of the simulation is to find the required height of the injection frequency at which the magnetizing inductance does not influence the calculation of σL_S. Here, the IM is supplied by a sinusoidal single phase voltage at varying frequencies. As no saturation is considered in the model, the amplitude (U_{S0}) and the DC-offset (U_{S1}) do not influence the result.

The upper plot in figure 4.12 illustrates how the injection frequency influences the outcome of the calculation with 3.24. At the rated frequency of 16Hz the error in the calculation is already diminished to 0.7%. However, for IM with a higher leakage factor σ the curve can be less steep. In this case also the required frequency rises. As already mentioned, in literature there is no consent to which frequency should be used. The bottom plot shown the phase shift φ between the voltage and the current. Increasing the frequency results in a rising φ which slowly converges to 90°. Detecting a bigger phase shift is less susceptible to small errors. To conclude, the simulation shows that the frequency should be chosen from the rated frequency upwards.

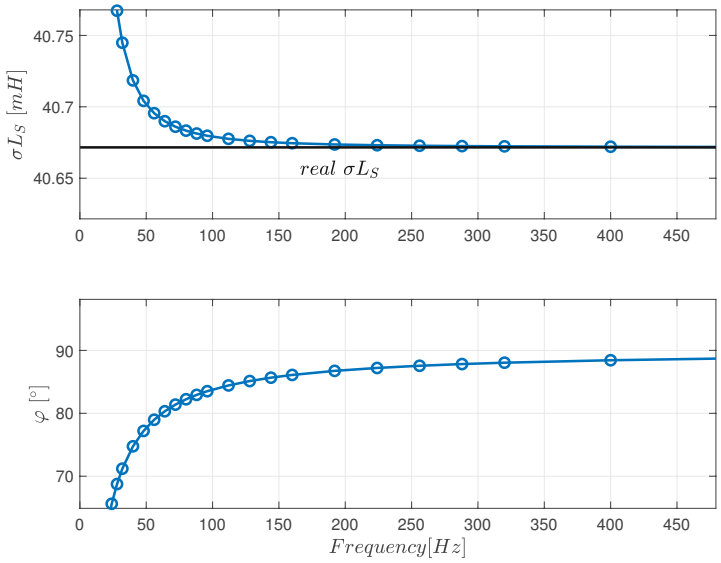

Figure 4.12: This figure shows calculated σL_S in relation to the injection frequency in the upper plot. The lower plot shows the corresponding phase shift between the voltage and the current. The curves were recorded in simulink.

Experimental Environment

Frequency To verify the information gained in the simulation, a variable frequency test was conducted. Assuming that the current controller is not yet initialized, a SP voltage is applied to the machine. Staring at only a view percent of the rated voltage, U_{S0} is increased till the rated current $\hat{I_N}$ flows. Then U_{S1} is adjusted at each frequency to produce a current amplitude of 1A or $0,056 \cdot \hat{I_N}$. Applying this signal to the IM, the following plot was obtained.
At a high DC-injection, the motor is highly saturated and thus leading to a much smaller inductance than in the simulation. Further, the calculated inductance continues to grow smaller even up till 200Hz. From $3xf_N = 48Hz$ the curve starts to become almost linear. Thus it is believed that this is the result of frequency dependent effects in the rotor bars.
Using the inverter measurements, results in a higher phase shift as the samples are not taken at the same time. At 200Hz the phase shift is already above 90°. One controller

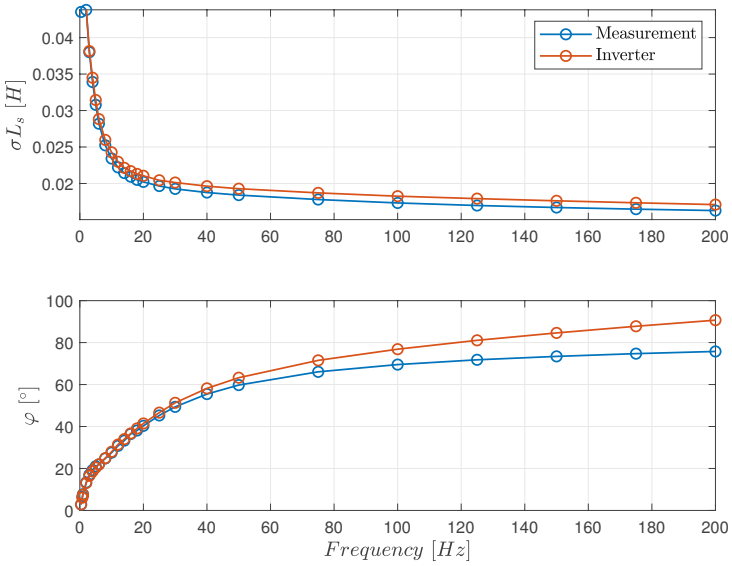

Figure 4.13: This figure shows calculated σL_S in relation to the injection frequency in the upper plot. The lower plot shows the corresponding phase shift between the voltage and the current. The blue curves are computed from DAQ measurements whereas the red ones are the result of the inverter data. Due to the asynchronous current measurement of the inverter, the calculated phase shift exceeds 90°at 200Hz.

cycle lasts 62,5μs. When a certain voltage is set, it is applied one cycle later. After another cycle the measured current is recorded. Thus leading to a minimum offset of 125μs. In addition the current is filtered which causes another delay. To increase the methods accuracy, this dead time needs to be compensated. This delay is constant and only dependent on the inverter. Using the delay at 1-200Hz the following plot can be obtained. Figure 4.14 shows a linear curve of $\Delta\varphi$ which is calculated at each frequency as:

$$\Delta\varphi = \varphi_{Inverter} - \varphi_{Measurement} \tag{4.6}$$

The fluctuations at the low frequencies come from the small time difference which makes the phase shift detection more prone to error.
Using this observation a linear function that fits to 4.14 is used to compensate the asynchronous sampling of the inverter. Hence figure 4.15 is drawn. It can be observed that the phase shift now coincides much better the DAQ measurements. In numbers, the error can be reduced from 4,7% to 1,14%.(calculated at 50Hz) The remaining error originates from the difference between the reconstructed voltage and real one. Nevertheless, the remaining deviation is small enough to be neglected.

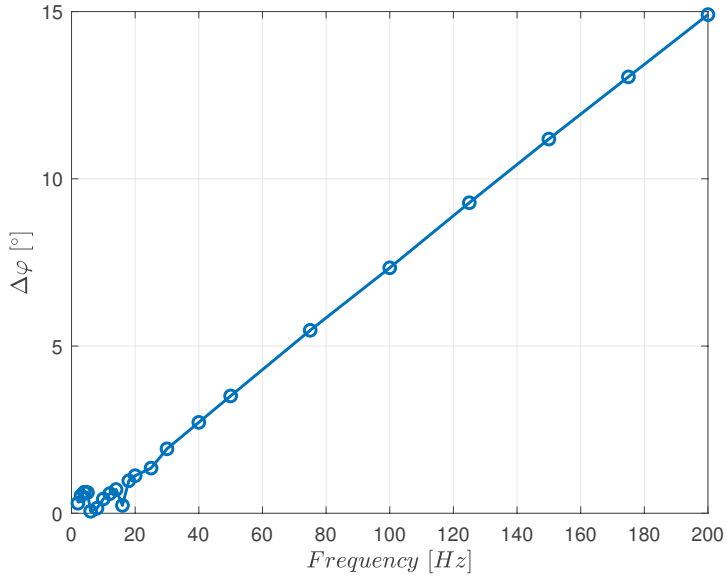

Figure 4.14: The difference between the measured DAQ phase shift and the inverter phase shift $\Delta\varphi$ is depicted in relation to the injection frequency.

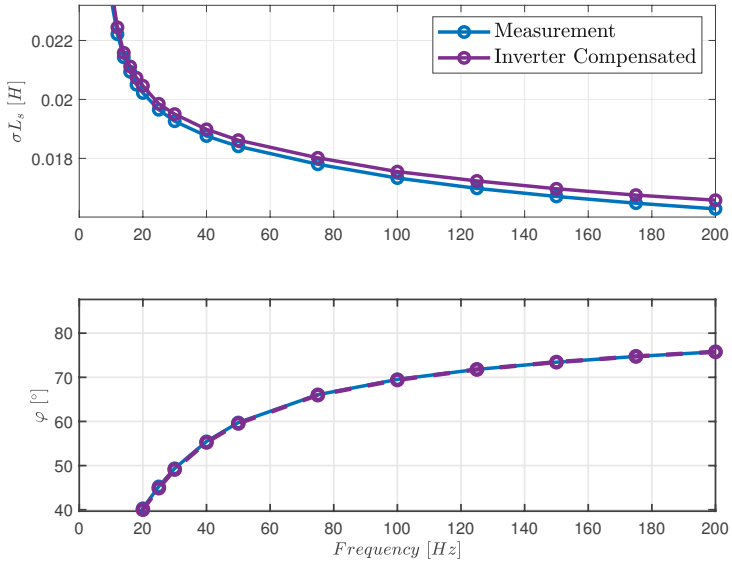

Figure 4.15: Compensated inverter measurements and DAQ measurements.

Saturation Although the transient inductance is often considered as constant, it also shows saturation effects. Two options are available to obtain the saturation characteristic with this test. The first is to apply a SP voltage with a varying DC component. In the second one, the DC component is set to zero while the amplitude is changed.

Applying the first method with a current amplitude of 1A($0.056 \cdot \hat{I_N}$) at 48Hz, σL_S is calculated at differing I_{S0} values. Figure 4.16 shows the result of this test. Where the measurements were obtained using the DAQ.

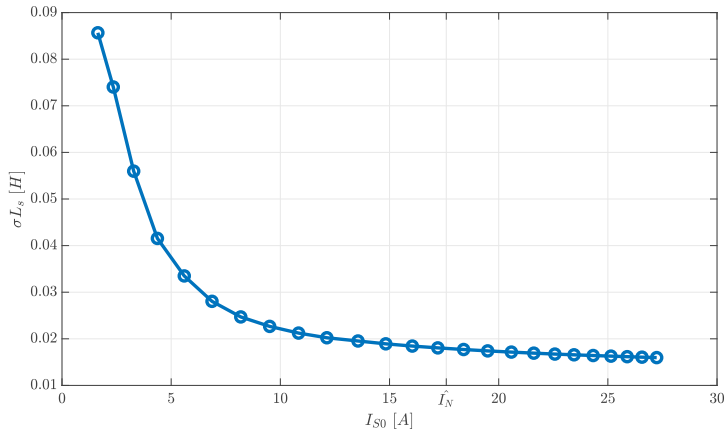

Figure 4.16: Transient inductance with DC-saturation at 48Hz.

The second method was also evaluated at an injection frequency of 48Hz. Figure 4.17 shows its outcome. With rising I_{S1}, the saturation is also clearly visible.

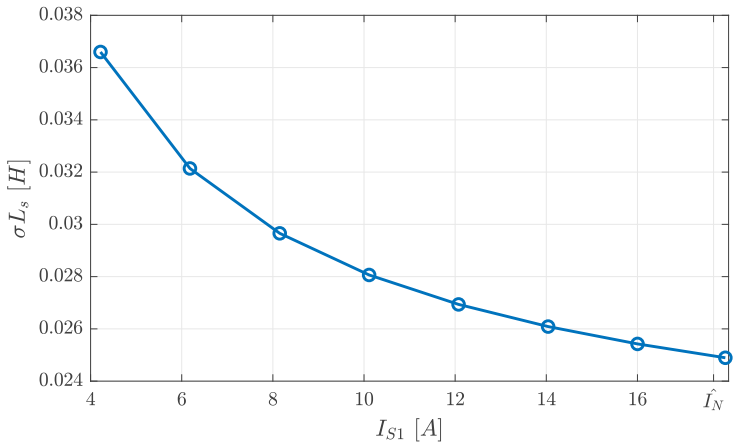

Figure 4.17: Transient inductance with AC-saturation at 48Hz.

Comparing the two methods is a difficult task, as the conditions in the IM are very different. An observation can be made though, that the values of the DC-saturated inductance are lower than those of the amplitude variation. This is the result of the varying saturation level in method 2 whereas in method 1 the produced flux only fluctuates with a much smaller amplitude.

Space Angle Additionally the method with the DC-offset was tested for its dependence on the chosen space angle ϑ. With $I_{S0} = \hat{I_N}$ and $I_{S1} = 1A$ at 48Hz, the transient inductance is calculated for $\vartheta = 0° - 360°$. The result is shown in 4.18. Compared to the mean value, the maximum deviation of the whole set is 1.34%. Therefore it can be assumed that choosing a particular space angle is not necessary. This means that the most convenient ϑ can be used.

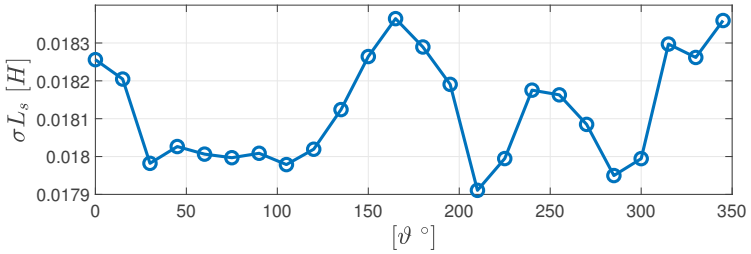

Figure 4.18: Dependence of the transient inductance on the space angle ϑ. σL_S is obtained using a single phase excitation at 48Hz with $I_{S0} = \hat{I_N}$ and $I_{S1} = 1A$.

4.7 Magnetizing Inductance

4.7.1 Low Frequency Single Phase Excitation

Using the low frequency injection method in the simulation, and calculating the magnetizing inductance, figure 4.19 can be drawn. The small fluctuations are likely due to errors produced by the FFT for amplitude and phase reconstruction. As the known transient inductance and stator resistance are utilized in the calculation the outcome is rather accurate over the whole frequency range. However, σL_S is not constant in the real IM and depends on the saturation level. Thus to validate this method, the simplified simulation is not enough and the real IM needs to be considered.

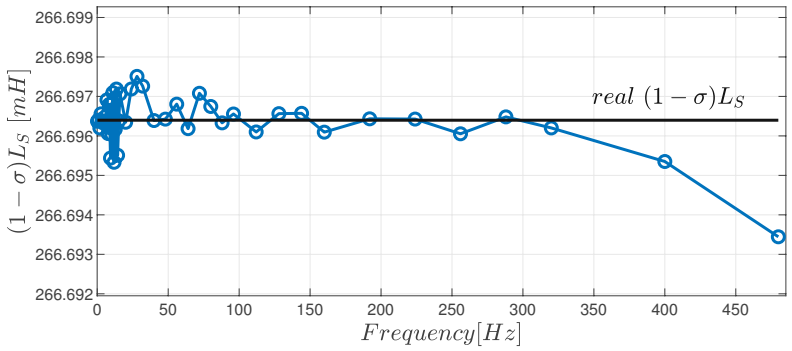

Figure 4.19: Simulation results from the low frequency single phase test

Experimental Environment

Identifying the magnetizing inductance with the proposed method proofed to be a lot more difficult as seen with in the simulation. The saturation characteristic was obtained by choosing the frequency according to condition 3.29. Inserting the parameters from the nameplate estimation shows that f should be below 0.98Hz. Therefore, the frequency was chosen to be 0.5Hz. The AC current amplitude is 1A and the DC component is varied. For the determination of $(1-\sigma)L_S$ the identified $R_S = 1.9531\Omega$ from 4.5 and the corresponding values of the transient inductance at the different saturation states from 4.17 are used. In figure 4.20 the result is illustrated. The typical saturation curve can be observed. However the calculated value of the magnetizing inductance is far below the values of the IEEE and the transient test.

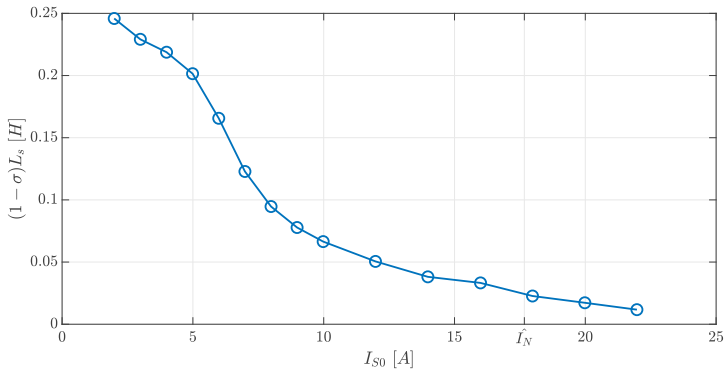

Figure 4.20: This figure shows the saturation curve of $(1-\sigma)L_S$ obtained with the low frequency test by varying the DC current component.

A different approach was also tested. The DC current is kept at $I_{S0} = 0$ and the AC component I_{S0} is varied. Whereas the same frequency (0.5Hz) as above is injected. This test is proposed in [20] and also utilizes equation 3.28 to calculate the magnetizing inductance. Figure 4.21 shows the outcome of the DAQ-measurements using $R_S = 1.9531\Omega$ and again the corresponding values of the transient inductance at the different saturation states from 4.17. As mentioned in literature the inductance is larger than the actual one. In normal operating conditions, the flux level inside the motor is kept constant whereas here the level keeps changing with the injected current. The drop at low saturation levels is due to the inverter dead time which corrupts the measurements. In order to get appropriate values using this method using the inverter, a dead time compensation is required. This is also suggested in [20].

A major drawback of using equation 3.28 to calculate the $(1-\sigma)L_S$ is the reliance on the estimation of other parameters. As the injection frequency is chosen very low, errors due to a wrong transient inductance can be neglected. However the stator resistance heavily influences the outcome. This is illustrated in figure 4.22 where the saturation curve from figure 4.20 is redrawn for different stator resistances. Considering that $R_S = 1.9\Omega$, a small error of +-5% in the stator resistance results in an error of -26% or +32%. The stator resistance is further dependent on the temperature of the stator windings which can cause errors at high DC currents.

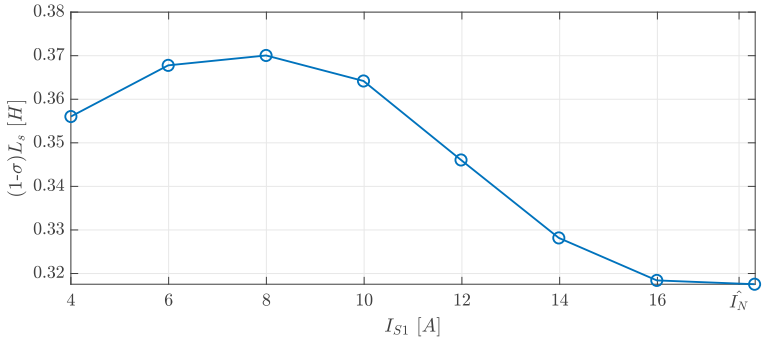

Figure 4.21: This figure shows the saturation curve of $(1-\sigma)L_S$ obtained with the low frequency test by varying the AC current component.

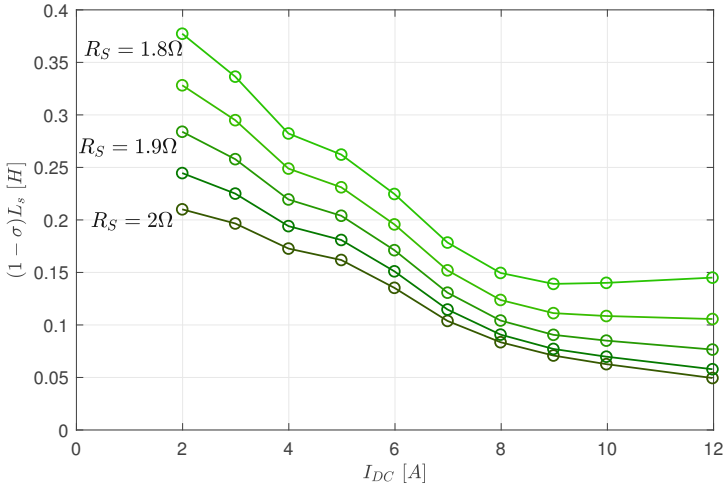

Figure 4.22: Error propagation due to a false estimate of R_S

4.7.2 Transient Test

For the evaluation of the transient test of the magnetizing inductance, no simulation results are presented, as the method relies highly on the voltage drop over the IGBTs and diodes after the null voltage vector is set. The test is conducted at a space angle $\vartheta = 90°$ and the currents and voltages are obtained trough the DAQ. Figure 4.23 shows the voltage and current curves after the voltage is set to zero. It can be observed that the voltage drops over the semi conductors are significant. Thus requiring accurate knowledge of the voltages in order to calculate the inductance.

When choosing different current levels before the transient, a saturation characteristic can be obtained. This is illustrated in figure 4.24 where the stator inductance is calculated at currents ranging from 2-19A. When also using the voltage in equation 3.32 a realistic saturation curve is obtained. This curve is also in close agreement to the one obtained with the classic IEEE test.[9] However using only the current results in a much lower value with a huge error. For accurate results the characteristics of the IGBTs need to be taken into account.

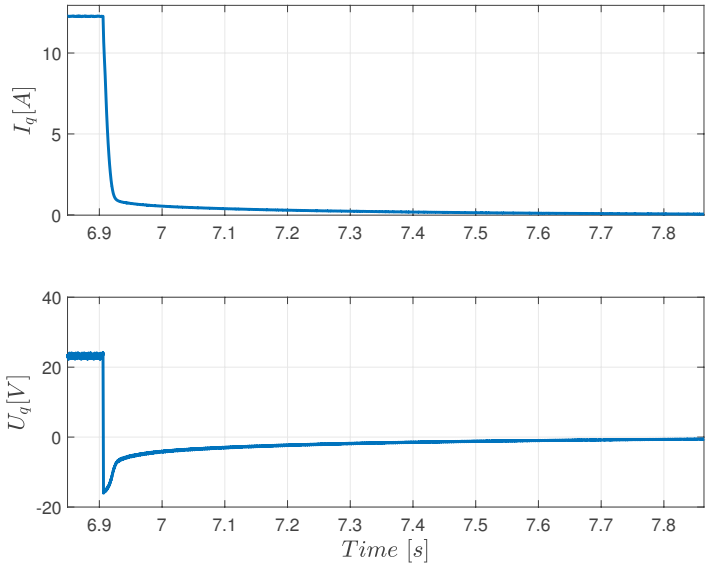

Figure 4.23: The upper plot shows the current decay after the null voltage vector is applied. In the lower picture the corresponding voltage is shown.

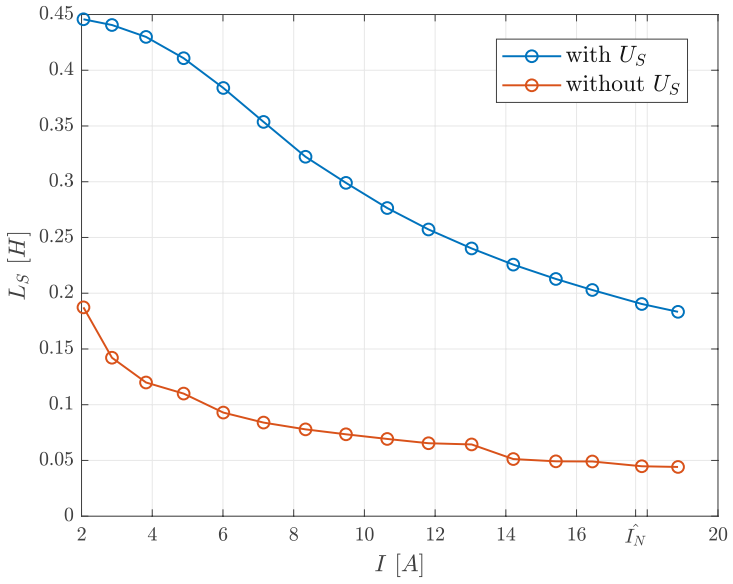

Figure 4.24: The calculated inductance L_S is shown for differing DC current levels before the transient. Leading to this saturation curve. The inductance is shown with and without using the voltage drops over the semiconductors.

As the motor is supplied with at $\vartheta = 90°$ only phase 2 and 3 are conducting. After the zero voltage vector is applied the path of the current goes through one switch and one free wheeling diode. Hence, u_S in equation 3.32 can be described as [21]:

$$u_S = \frac{u_d + u_t}{2} \tag{4.7}$$

where u_d is the threshold voltage of the diode and u_t the IGBT voltage drop. These voltage drops can either be determined using the data sheets or by performing a test once with additional measurement equipment and storing the data in a lookup table.[35] also suggests a self identification of the non linearities using voltage steps. Here the voltage drop is obtained using a one time measurement with the DAQ. Applying a DC-current and then measuring the voltage and currents after the null vector is applied. Figure 4.25 shows the result using a lookup table for the semiconductor voltage drops.

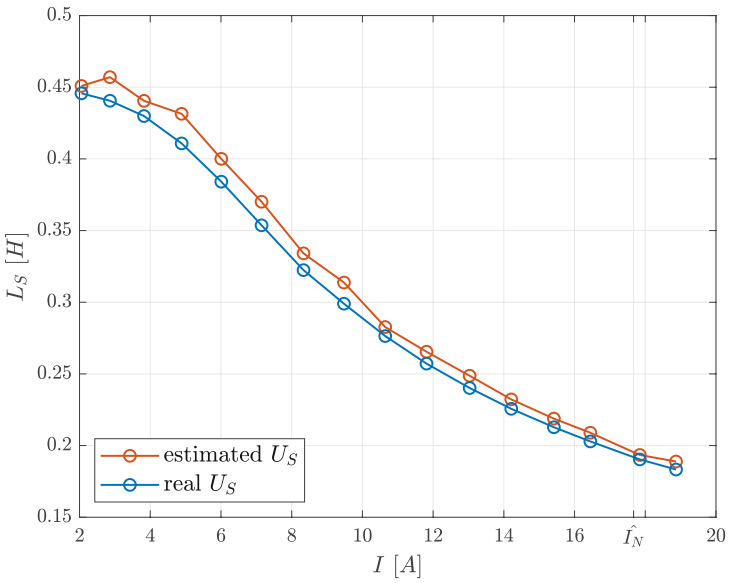

Figure 4.25: The calculated inductance L_S is shown for differing DC current levels before the transient. For the blue curve the measured voltage is taken whereas for the red curve the stator voltage is estimated with a lookup table.

4.8 Rotor Resistance

For identification of the rotor resistance, the low frequency test is evaluated. In the simulation, R'_R could be determined with an error below 1%. Due to its dependence on the frequency and temperature, identifying the rotor resistance in real is more complicated. R'_R is usually given at 20°. Therefore the measurement should be taken at this temperature. If this is not possible due to the surrounding environment, the temperature must be measured. Then the value at 20°can be estimated by using the temperature coefficient α and the temperature difference ΔT. The temperature coefficient must be chosen according to the material of the rotor bars which is mostly copper or aluminium.

$$R'_R(T = 20°) = \frac{R'_R}{1 + \alpha \cdot \Delta T} \tag{4.8}$$

In order to satisfy equation 3.33, the injection frequency was chosen at 0.5Hz. The DC current component I_{S0} should be just high enough so that the inverter non linearities do not effect the superimposed AC signal. With the already identified R_S and the voltage drop seen in figure 4.6, the minimum current can be calculated as,

$$I_{S0,min} = \frac{\Delta U}{R_S} = \frac{15.25V}{1.9928\Omega} = 7.6525A \tag{4.9}$$

Where ΔU is calculated using the current and the inverter voltage at the first step of the R_S DC-test.

$$\Delta U = U_{S0} - R_S \cdot I_{S0} \tag{4.10}$$

In addition the amplitude of the AC component must be added. Here $I_{S1} = 1A$ leads to a minimum DC component of $I_{S0} = 8.6525A$. To be on the safe side the test was conducted at $I_{S0} = 10A$ and $I_{S1} = 1A$. Using this input, the estimated R_S value and the value of the estimated transient inductance at 10A saturation R'_R was obtained as 0.871Ω with DAQ-measurements and 0.654Ω with the inverter. According to the data provided by the manufacturer, R'_R at 20°should be 0.889Ω. Thus resulting in an error of 2% or 26.4%.

4.9 Rotor Time Constant

4.9.1 Single Phase Current Injection Strategy

Simulation

As the proposed method suggests, the model is supplied by a sinusoidal single phase current with the amplitude being the rated current. ($I_{S1} = \hat{I_N}$) After a couple periods the signal with the frequency f, get switched to peak value of the rated magnetizing current.($I_{S0} = \hat{I_M}$) If at the switching instant the actual magnetizing current does not equal I_{S1} a voltage transient appears. This transient is recorded directly at the output of the current controller. By applying this signal to the simulink model and varying the injection frequency, figure 4.26 can be drawn. It can be seen that Δu of the voltage transient is in the range of a couple volts. Hence, the use of the voltage time area is recommended to reduce the influence of noise. The recording of the transient was found to be accurate when starting at the point where the stator current reaches the desired DC value. Taking into account any measurements before that instant, can lead to errors due to the current controller overshoot. At the frequency where the transient disappears ($\Delta u = 0$,$\Delta A = 0$), the rotor time constant is calculated. In the simulation, the method proofs to be very accurate with an error below 1%.

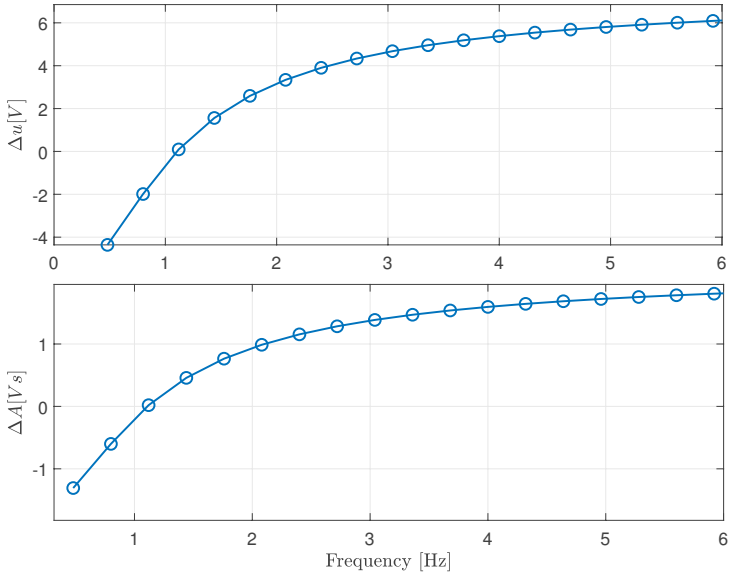

Figure 4.26: These curves were obtained in the simulation. For the varying frequencies at the same amplitude, the top plot shows the difference Δu between the start and the end of the voltage transient. In the bottom plot the corresponding voltage time area is displayed.

Experimental Environment

The same test as in the simulation was conducted through the inverter. By calculating ΔA at different frequencies, the curves in figure 4.27 were obtained. Looking at the

green and blue curves where the amplitude is $\hat{I_N}$ and the DC current value is $\hat{I_M}$, a difference can be seen at lower frequencies. At those lower frequencies, the magnetizing current is to high at the switching instant. Therefore, the IM is in a saturated state. Due to the saturation the actual magnetizing current cannot reach much higher values. Thus, leading to the flattening of the transient at lower frequencies.

When the rated magnetizing current is unknown it has to be estimated with the nameplate data. For this IM the estimated value is slightly lager than the value known from the manufacturer. By conducting the test with the estimated $\hat{I_M}$ the red curve in figure 4.27 can be drawn. It can be seen that the higher saturation state leads to a smaller ΔA at low frequencies. Furthermore, the frequency with no transient is also smaller.

τ_R is then calculated by interpolating between the two points closest to $\Delta A = 0$. This leads to the rotor time constant estimates of 296ms using the manufacturers $\hat{I_M}$ and 278ms using the nameplate estimate. From data provided by the manufacturer τ_R should equal 300ms. Hence using the correct DC current leads to an error of 1,33%. Using the nameplate estimate, the error equals 7,33%. However it should be noted that when the motor is operated at the estimated magnetizing current, the required τ_R is also different and most likely closer to the second value.

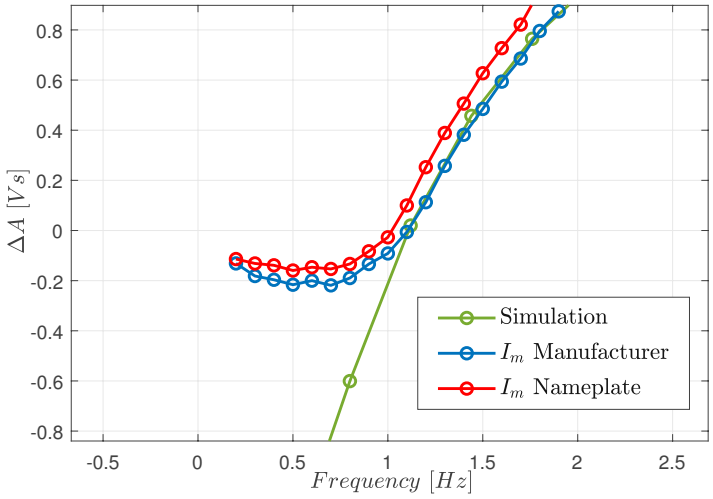

Figure 4.27: ΔA of the voltage transient at different frequencies. In the simulation(green) and the blue curve the DC current value equals the magnetizing current from the manufacturers data whereas in the red curve its nameplate estimate was utilized.

An interesting observation could be made when conducting the method with variable frequencies, at $I_{S1} = \hat{I_N}$, $\hat{I_M}$ from the manufacturers data and at two different space angles $\vartheta = 0°$ and $\vartheta = 90°$. This is illustrated in figure 4.28. Applying the signal at $\vartheta = 0°$ results in a bigger voltage transient at low frequencies. However, the identified τ_R are the same for both angles. This behaviour could be explained by the different pathways of the magnetic field. At $\vartheta = 90°$, only two phases are conducting whereas at

$\vartheta = 0°$ all three phases hold a current. As seen in the plot, a bigger transient means a steeper zero crossing of $\Delta A(f)$. This reduces the difficulty of finding $\Delta A(f) = 0$ and increases the methods accuracy. Therefore, using $\vartheta = 0°$ is recommended here.

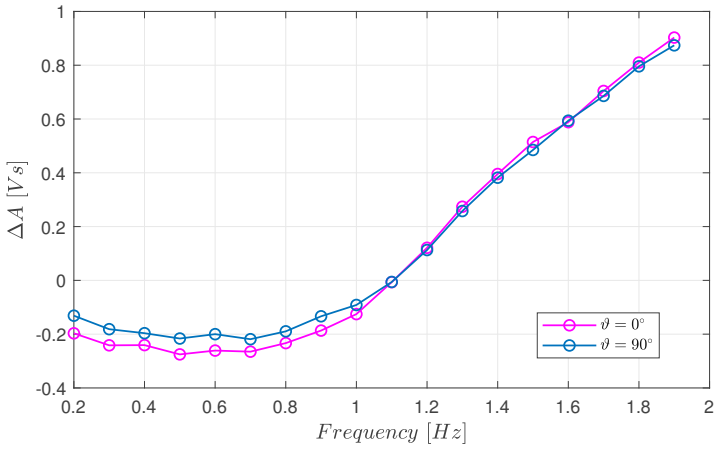

Figure 4.28: ΔA of the voltage transient at different frequencies. The two curves were obtained using different space angles for injection.

To proof the concept of this method, the test was also conducted at the rated slip frequency obtained from the nameplate data (f=1,366Hz) and a variable amplitude. Figure 4.29 illustrates ΔA at these amplitudes. Here τ_R calculates to 295ms, which is almost the same as when the frequency is varied. Thus validating that both methods are applicable. The drawback of this method is that when the slip frequency estimate is high, a high amplitude is required. This excessive current could lead to heating of the windings and corrupt the identification of the rotor time constant.

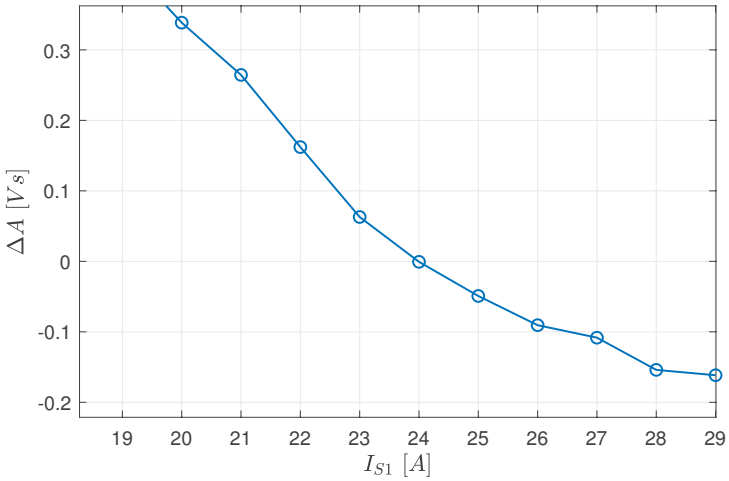

Figure 4.29: ΔA of the voltage transient at different amplitudes and the rated slip estimated from the nameplate. For comparison, the rated current $\hat{I_N} = 17.67A$.

4.9.2 Flux Observer based Strategy

The method described in 3.8.2 is first tested in simulink and then evaluated with the experimental setup.

Simulation

The sequence described in 3.9, with the first step $I_{S0} = \hat{I_N}$, the second $I_{S0} = -\hat{I_N}$ and the third being $I_{S0} = -\hat{I_M}$ was applied to the model. By varying the rotor time constant estimate $\hat{\tau_R}$ and measuring ΔA, the figure below could be obtained. The estimate of $\hat{\tau_R}$ directly influences the time, the negative current step is applied. At high $\hat{\tau_R}$, the magnetizing current already equals the stator current before the last step is set. Hence, the voltage transient will not get bigger. This can be seen in the figure for $\hat{\tau_R} > 470ms$. As the simulation is a very simplified model, the time constant that was found via this method possesses an error below 1%. Another observation could be made from the simulation. The higher the current steps, the steeper is the curve shown in figure 4.30. This is logical considering that i_m is described here as a first order delay or an exponential function. The slope of the exponential function is higher for a lager difference between the fist and the second current step. Thus resulting in a larger difference of $i_m - \hat{i_m}$ for the same differing time constant estimate.

Experimental Environment

By injecting the same sequence as described in the simulation, the following plot could be obtained.

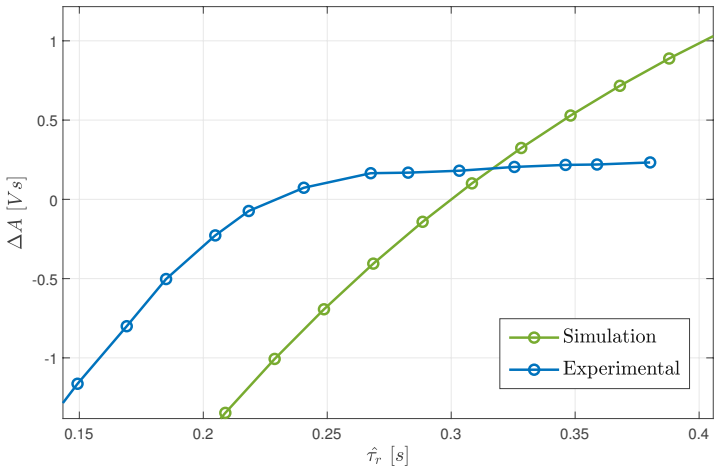

Figure 4.30: ΔA of the voltage transient using different $\hat{\tau_R}$. Using the same input sequence ($\hat{I_N}$,$-\hat{I_N}$,$-\hat{I_M}$) in the simulation and the test using the inverter.

The identified time constant from the test ($\tau_R = 230ms$) differs widely from the one in the simulation($\tau_R = 300ms$). Since the test is short enough to rule out the influence of the temperature, the huge difference must originate from the saturation of the IM. Therefore the test was repeated using the following step sequence, using the RMS value

of the rated current instead of the amplitude. I_N,$-I_N$,$-\hat{I_M}$. This results in a time constant at $\Delta A = 0$ of $\hat{\tau_R} = 275ms$. Nevertheless closer to the manufacturer value, the estimate still has an error of 8.3%. After further study it was found that the height of the first current step is responsible for the wrong estimate. As the magnetizing current reaches the value of the stator current in the first step, the height of the first step needs to equal the rated magnetizing current $\hat{I_M}$. Doing otherwise, leaves the IM in a higher saturated state than in real operations, leading to the smaller τ_R. Hence the step sequence needs to be changed to $\hat{I_M}$,$-\hat{I_N}$,$-\hat{I_M}$. Whereas the second step does not influence the outcome of the method. It effects the slope of the curves in figure 4.30. The higher the current, the steeper is the zero crossing point. Figure 4.31 shows the outcome of the changed input sequence. The results of the simulation and the experimental ones, are now comparable. As expected the transient or ΔA is lower at high $\hat{\tau_R}$ due to the saturation of the IM. Nevertheless, the rotor time constant was identified using interpolation as $\tau_R = 308ms$. This equals an error of only 2.7% in comparison to the manufacturers data.

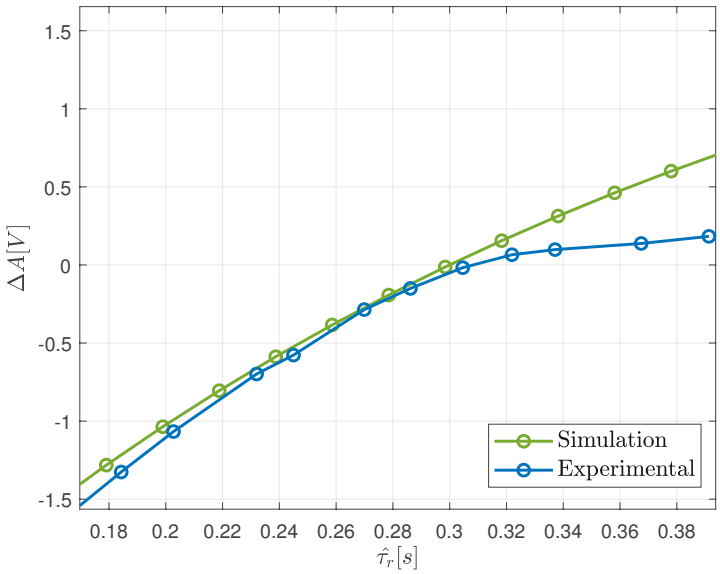

Figure 4.31: ΔA of the voltage transient using different $\hat{\tau_R}$. Using the new input sequence ($\hat{I_M}$,$-\hat{I_N}$,$-\hat{I_M}$) in the simulation and the test using the inverter.

CHAPTER 5

Conclusion

In this thesis, identification methods for induction motors at standstill are studied. An introduction on IMs is given with the mathematical model using space phasors. The T and inverse-Γ equivalent circuits are introduced and the general drive structure is discussed.

A great number of standstill parameter identifications have already been developed and are available in literature. A review of existing methods is provided. Several methods which do meet the requirements of self-commissioning and can be implemented without the need of excessive computational power, were chosen for further investigation. The methods are first described in detail and then investigated using a simulation. In addition, test were conducted on a 4,6kW IM using an inverter as power supply.

To identify the stator resistance, the well established two step DC test was conducted. In both the simulation and the measurements the results were rather accurate. Hence, no other method was considered.
In order to identify the transient inductance of the motor which is required for the current controller in the field oriented control, two methods are studied. The first one is based on applying a positive and then a negative voltage pulse to the IM. This method proofed to be valid in the simulation. However, due to the inverter dead time effects the current rise is slowed resulting in an erroneous parameter. In order to cope with this error and to provide additional information about the saturation of the inductance, a test using current steps is introduced. Several current controlled steps are applied and the transient inductance is calculated with the CC parameters and the current response. It was observed that the right tuning of the CC is crucial to the accuracy of this method. Leaving the method to be very dependent on these settings. Additional measurements need to be conducted using the proposed settings with an iterative approach or by using only a proportional element. The second method is based on a high frequency single phase injection. Thereby a DC component superimposed on the AC signal is used to get different saturation states of the motor. In addition, the

DC component reduces the effect of the error produced by the reconstructed voltage, as only the AC signals are required for the calculations. Another advantage of this method is that the CC does not need to be tuned beforehand. Furthermore, it was shown that the asynchronous measurement of the current and the reconstructed voltage can be compensated when the delay is known.

For the identification of the magnetizing inductance two methods were chosen for investigation. Both require already estimated values of the transient inductance and the stator resistance. In the first method a DC current is applied and then a null voltage vector is set. Integrating the current and voltage transients provides the value of the magnetizing inductance. Measurements with the DAQ-system showed that by applying different DC currents an accurate value of the inductance can be determined. As the voltage transient is cased by the voltage drops over the inverters semiconductors, $u_S(i_S)$ for the specific space angle needs to be obtained in order to conduct the test only with the inverter. To obtain this curve, one measurement of the transient starting from a high DC level with the DAQ-system was recorded and stored in a lookup table. The lookup table is only dependent on the inverter semiconductors and if once determined can be used to test any motor. It should also be mentioned that the $u_S(i_S)$ is only valid at a specific space angle. Using the lookup with the measurements of the inverter provided an accurate result. In the second method, a sinusoidal single phase current is applied and the inductance is calculated with the voltage amplitude, current amplitude and their phase shift. Conducting the test with a superimposed DC signal resulted in an estimate of the inductance that is much lower than the one that was obtained with the IEEE or transient test. The reason for this could be that the motor is in higher saturated state than in normal operation. Therefore, the test was also performed without a DC component at various amplitudes. As already stated in literature the identified inductance is larger than the actual one. It was also found that in the low amplitude region, the estimate becomes erroneous due to the inverters non linearities. Thus a dead time compensation is required to provide accurate results.
The rotor resistance refereed to the stator was identified with a low frequency single phase test. It was found that a minimum DC offset can be calculated to be able to neglect the inverter dead time effects. The result however still proved erroneous as the temperature could not be measured during this test. To provide a reasonable statement about the accuracy of this method, this needs to be taken into account.

At last two methods for the direct estimation of the rotor time constant are introduced. Due to the possibly inaccurate determination of the rotor resistance and the magnetizing inductance, identifying the rotor time constant directly provides a considerable alternative. Whereas both methods rely on the same physical principle, they differ in there injection strategy. The goal is to reduce a seen voltage transient below a detectable value. The first one applies a sinusoidal single phase current and after a steady state is reached switches to a DC value which equals the desired magnetizing current. Depending on the amplitude and frequency of the AC signal, a positive or negative voltage transient appears after the switching instant. It was found that varying the amplitude or the frequency both result in the same τ_R estimate. However, varying the frequency proofed to be the safer option. Setting the frequency too high can result

in a very high current amplitude at the point the voltage transient disappears. In second method first a positive DC current is applied which is then switched to the negative rated current. A flux observer with a initial time constant estimate is used to estimate the magnetizing current. When the estimated magnetizing current reaches the negative rated magnetizing current, the injection is then switched to the negative rated magnetizing current. If the estimate is right no voltage transient should appear. The tests showed that setting the first DC current to the rated current saturates the motor too much and leads to a false identification. Therefore, the value was changed to the positive magnetizing current. Using this changed sequence, an accurate estimate could be made. Both Methods provide an identified rotor time constant with an error below 3% in comparison to the manufacturers data. The second method provides a slightly larger estimate whereas using the first method results in a lower estimate. An advantage of the sinusoidal test is, that the slope of ΔA is steeper at the point where τ_R is identified. This can result in better accuracy when the measurements are evaluated using the inverters controller instead of MATLAB. In this thesis the rotor time constant was determined by performing the methods at many points and then interpolating between the two values where the transient is closest to zero. To speed up the identification process an iterative approach could be used in future works.

Bibliography

[1] P. C. Sen, *Principles of electric machines and power electronics*. John Wiley & Sons, 2007.

[2] R. Browning, "Evolution of induction motors-the ever-shrinking motor," *IEEE Industry Applications Magazine*, vol. 3, no. 1, pp. 16–, Jan. 1997.

[3] V. Donescu, A. Charette, Z. Yao, and V. Rajagopalan, "Modeling and simulation of saturated induction motors in phase quantities," *IEEE Transactions on Energy Conversion*, vol. 14, no. 3, pp. 386–393, Sep. 1999.

[4] H. A. Toliyat, E. Levi, and M. Raina, "A review of rfo induction motor parameter estimation techniques," *IEEE Transactions on Energy Conversion*, vol. 18, no. 2, pp. 271–283, Jun. 2003.

[5] A. Hughes and W. Drury, *Electric motors and drives: fundamentals, types and applications*. Newnes, 2013.

[6] S. A. Odhano, P. Pescetto, H. A. A. Awan, M. Hinkkanen, G. Pellegrino, and R. Bojoi, "Parameter identification and self-commissioning in AC motor drives: a technology status review," *IEEE Transactions on Power Electronics*, p. 1, 2018.

[7] K. P. Kovács and I. Rácz, *Transiente vorgänge in Wechselstrommaschinen*. Verlag der ungarischen Akademie der Wissenschaften, 1959, vol. 1.

[8] M. Schrödl, "Unterlagen zur vorlesung elektrische antriebe," Institut fÃ¼r Energiesysteme und Elektrische Antriebe, 2013.

[9] "IEEE standard test procedure for polyphase induction motors and generators," *IEEE Std 112-2017 (Revision of IEEE Std 112-2004)*, pp. 1–115, Feb. 2018.

[10] J. Godbersen, "A stand-still method for estimating the rotor resistance of induction motors," in *Proc. Conf. Record of the 1999 IEEE Industry Applications Conf.. Thirty-Forth IAS Annual Meeting (Cat. No.99CH36370)*, vol. 2, Oct. 1999, pp. 900–905 vol.2.

[11] S. A. Odhano, "Self-commissioning of ac motor drives," Ph.D. dissertation, Politecnico di Torino, 2014.

[12] J. K. Pedersen, F. Blaabjerg, J. W. Jensen, and P. Thogersen, "An ideal PWM-vsi inverter with feedforward and feedback compensation," in *Proc. Fifth European Conf. Power Electronics and Applications*, Sep. 1993, pp. 501–507 vol.5.

[13] A. R. Munoz and T. A. Lipo, "On-line dead-time compensation technique for open-loop PWM-vsi drives," *IEEE Transactions on Power Electronics*, vol. 14, no. 4, pp. 683–689, Jul. 1999.

[14] Y. Murai, T. Watanabe, and H. Iwasaki, "Waveform distortion and correction circuit for PWM inverters with switching lag-times," *IEEE Transactions on Industry Applications*, vol. IA-23, no. 5, pp. 881–886, Sep. 1987.

[15] R. B. Sepe and J. H. Lang, "Inverter nonlinearities and discrete-time vector current control," *IEEE Transactions on Industry Applications*, vol. 30, no. 1, pp. 62–70, Jan. 1994.

[16] M. Haque, "Determination of nema design induction motor parameters from manufacturer data," *IEEE transactions on Energy conversion*, vol. 23, no. 4, pp. 997–1004, 2008.

[17] A. Boglietti, A. Cavagnino, and M. Lazzari, "Computational algorithms for induction-motor equivalent circuit parameter determination-part i: Resistances and leakage reactences," *IEEE Transactions on Industry Applications*, vol. 58, no. 9, pp. 3723–3733, 2011.

[18] P. Vas, *Parameter estimation, condition monitoring, and diagnosis of electrical machines*. Clarendon Press ; Oxford University Press Oxford : New York, 1993.

[19] K. Wang, W. Yao, B. Chen, G. Shen, K. Lee, and Z. Lu, "Magnetizing curve identification for induction motors at standstill without assumption of analytical curve functions," *IEEE Transactions on Industrial Electronics*, vol. 62, no. 4, pp. 2144–2155, Apr. 2015.

[20] S. A. Odhano, A. Cavagnino, R. Bojoi, and A. Tenconi, "Induction motor magnetizing characteristic identification at standstill with single-phase tests conducted through the inverter," in *Proc. IEEE Int. Electric Machines Drives Conf. (IEMDC)*, May 2015, pp. 960–966.

[21] L. Peretti and M. Zigliotto, "Automatic procedure for induction motor parameter estimation at standstill," *IET Electric Power Applications*, vol. 6, no. 4, pp. 214–224, Apr. 2012.

[22] A. Gastli, "Identification of induction motor equivalent circuit parameters using the single-phase test," *IEEE Transactions on Energy Conversion*, vol. 14, no. 1, pp. 51–56, Mar. 1999.

[23] N. R. Klaes, "Parameter identification of an induction machine with regard to dependencies on saturation," *IEEE Transactions on Industry Applications*, vol. 29, no. 6, pp. 1135–1140, Nov. 1993.

[24] S. Lee, A. Yoo, H. Lee, Y. Yoon, and B. Han, "Identification of induction motor parameters at standstill based on integral calculation," *IEEE Transactions on Industry Applications*, vol. 53, no. 3, pp. 2130–2139, May 2017.

[25] A. Bechouche, H. Sediki, D. O. Abdeslam, and S. Haddad, "Identification of induction motor at standstill using artificial neural network," in *Proc. IECON 2010 - 36th Annual Conf. IEEE Industrial Electronics Society*, Nov. 2010, pp. 2908–2913.

[26] ——, "A novel method for identifying parameters of induction motors at standstill using adaline," *IEEE Transactions on Energy Conversion*, vol. 27, no. 1, pp. 105–116, Mar. 2012.

[27] Y. Kwon, J. Lee, S. Moon, B. Kwon, C. Choi, and J. Seok, "Standstill parameter identification of vector-controlled induction motor using frequency characteristics of rotor bars," in *Proc. IEEE Industry Applications Society Annual Meeting*, Oct. 2008, pp. 1–7.

[28] A. H. Mabrek and K. E. Hemsas, "Transient operation modeling of induction machine using standstill frequency response test," in *Proc. 4th Int. Conf. Electrical Engineering (ICEE)*, Dec. 2015, pp. 1–6.

[29] M. Depenbrock and N. R. Klaes, "Determination of the induction machine parameters and their dependencies on saturation," in *Proc. Conf. Record of the IEEE Industry Applications Society Annual Meeting*, Oct. 1989, pp. 17–22 vol.1.

[30] J.-W. Choi and S.-K. Sul, "Inverter output voltage synthesis using novel dead time compensation," *IEEE Transactions on Power Electronics*, vol. 11, no. 2, pp. 221–227, Mar. 1996.

[31] J.-K. Seok, S.-I. Moon, and S.-K. Sul, "Induction machine parameter identification using PWM inverter at standstill," *IEEE Transactions on Energy Conversion*, vol. 12, no. 2, pp. 127–132, Jun. 1997.

[32] M. O. Sonnaillon, G. Bisheimer, C. D. Angelo, and G. O. Garcia, "Automatic induction machine parameters measurement using standstill frequency-domain tests," *IET Electric Power Applications*, vol. 1, no. 5, pp. 833–838, Sep. 2007.

[33] M. Carraro and M. Zigliotto, "Automatic parameter identification of inverter-fed induction motors at standstill," *IEEE Transactions on Industrial Electronics*, vol. 61, no. 9, pp. 4605–4613, Sep. 2014.

[34] R. J. Kerkman, J. D. Thunes, T. M. Rowan, and D. W. Schlegel, "A frequency-based determination of transient inductance and rotor resistance for field commissioning purposes," *IEEE Transactions on Industry Applications*, vol. 32, no. 3, pp. 577–584, May 1996.

[35] M. Zigliotto, M. Carraro, and F. Tinazzi, "The influence of the squirrel cage rotor in the estimation of the im flux linkage at standstill," in *Proc. IEEE Int. Conf. Industrial Technology (ICIT)*, Feb. 2013, pp. 410–415.

[36] C. Wang, D. W. Novotny, and T. A. Lipo, "An automated rotor time-constant measurement system for indirect field-oriented drives," *IEEE Transactions on Industry Applications*, vol. 24, no. 1, pp. 151–159, Jan. 1988.

[37] S. Sheng, X. Cheng, H. Lu, W. Qu, and Y. Li, "An accurate rotor time constant estimation method for self-commissioning of multi-scale induction motor drives," in *Proc. IEEE Energy Conversion Congress and Exposition*, Sep. 2011, pp. 1700–1707.

[38] T. Wolbank, "Simulation elektrischer antriebe," Institut fÃ$\frac{1}{4}$r Energiesysteme und Elektrische Antriebe, 2009.

[39] A. Boglietti, P. Ferraris, M. Lazzari, and F. Profumo, "Induction motor equivalent circuit parameters determination from standard tests made with inverter supply," in *1993 Sixth International Conference on Electrical Machines and Drives (Conf. Publ. No. 376)*. IET, 1993, pp. 271–276.

[40] S.-K. Sul, *Control of electric machine drive systems*. John Wiley & Sons, 2011, vol. 88.

Appendix

Hiermit erkläre ich, dass die vorliegende Arbeit gemäß dem Code of Conduct, insbesondere ohne unzulässige Hilfe Dritter und ohne Benutzung anderer als der angegebenen Hilfsmittel angefertigt wurde. Die aus anderen Quellen direkt oder indirekt übernommenen Daten und Konzepte sind unter Angabe der Quelle gekennzeichnet.
Die Arbeit wurde bisher weder im In- noch im Ausland in gleicher oder in ähnlicher Form in anderen Prüfungsverfahren vorgelegt.

Wien, 13.5.2019

Christoph Pesendorfer